

MM1.5: METHODS, ANALYSIS & INSIGHTS FROM MULTIMODAL LLM FINE-TUNING

Anonymous authors

Paper under double-blind review

ABSTRACT

We present **MM1.5**, a new family of multimodal large language models (MLLMs) designed to enhance capabilities in text-rich image understanding, visual referring and grounding, and multi-image reasoning. Building upon the MM1 architecture, MM1.5 adopts a data-centric approach to model training, systematically exploring the impact of diverse data mixtures across the entire model training lifecycle. This includes high-quality OCR data and synthetic captions for continual pre-training, as well as an optimized visual instruction-tuning data mixture for supervised fine-tuning. Our models range from 1B to 30B parameters, encompassing both dense and mixture-of-experts (MoE) variants, and demonstrate that careful data curation and training strategies can yield strong performance even at small scales (1B and 3B).¹ Through extensive empirical studies and ablations, we provide detailed insights into the training processes and decisions that inform our final designs, offering valuable guidance for future research in MLLM development.

1 INTRODUCTION

Multimodal Large Language Models (MLLMs) have emerged as an increasingly active research topic in recent years. Closed-source models, such as GPT-4o (Islam & Moushi, 2024), GPT-4V (OpenAI, 2024), Gemini-1.5 (Team et al., 2023; Reid et al., 2024), and Claude-3.5 (Anthropic, 2023), have demonstrated remarkable capabilities in advanced multimodal understanding. Meanwhile, open-source models, such as the LLaVA series of work (Liu et al., 2023b;a; 2024a; Li et al., 2024c), InternVL2 (Chen et al., 2024b), Cambrian-1 (Tong et al., 2024a) and Qwen2-VL (Bai et al., 2023; team, 2024), are rapidly narrowing the performance gap. There has also been growing interest in developing models capable of understanding single-image, multi-image, and video data using a single set of model weights (Li et al., 2024c). Further discussion of recent works is in Appendix A.1.

Building upon MM1 (McKinzie et al., 2024), we introduce MM1.5, a new family of MLLMs carefully designed to enhance a set of core capabilities. Specifically, we focus on the following aspects.

- **OCR.** MM1.5 supports arbitrary image aspect ratios and resolutions of up to 4 Megapixels. By incorporating carefully selected OCR data to enhance text comprehension across different training stages, MM1.5 excels at understanding text-rich images.
- **Visual referring and grounding.** MM1.5 offers robust, fine-grained image understanding, extending beyond text prompts to interpret *visual* prompts such as points and bounding boxes. Moreover, MM1.5 can generate grounded responses by grounding text output with image bounding boxes. This capability is notably under-explored in most open-source models (*e.g.*, LLaVA-OneVision (Li et al., 2024c) and Phi-3-Vision (Abdin et al., 2024b)), and even in strong proprietary models like GPT-4o, which rely on set-of-mark (SoM) prompting (Yang et al., 2023) to reference image regions.
- **Multi-image reasoning.** MM1.5 benefits from large-scale interleaved pre-training, resulting in strong in-context learning and multi-image reasoning capabilities right out of the box. We further improve its capabilities via supervised fine-tuning (SFT) on additional multi-image data.

Our primary focus is on the most efficient model scales, 1B and 3B, together with their corresponding Mixture-of-Experts (MoE) variants, and demonstrates that even relatively small MLLMs can achieve competitive performance on various downstream tasks. Furthermore, we demonstrate that the

¹Additionally, we introduce two specialized variants: MM1.5-Video, designed for video understanding, and MM1.5-UI, tailored for mobile UI understanding, detailed in Appendix A.7 and A.8 correspondingly.

054
055
056
057
058
059
060
061
062
063
064
065
066
067
068
069
070
071
072
073
074
075
076
077
078
079
080
081
082
083
084
085
086
087
088
089
090
091
092
093
094
095
096
097
098
099
100
101
102
103
104
105
106
107

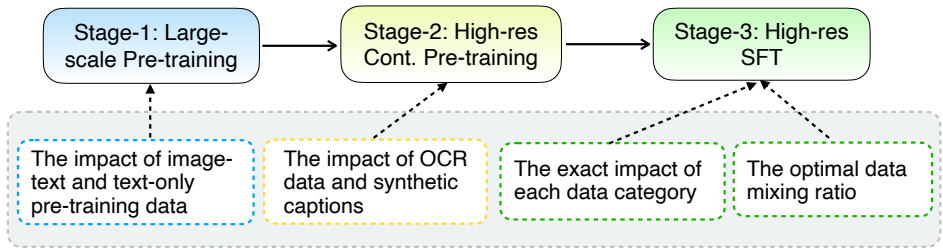


Figure 1: Recipe for building MM1.5. Model training contains three stages: (i) large-scale pre-training with low-resolution images (378×378), (ii) continual pre-training with high-resolution (up to 4 Megapixels) OCR data and synthetic captions, and (iii) supervised fine-tuning (SFT). At each stage, we aim to identify the optimal data mix and assess the impact of each data type.

MM1.5 recipe exhibits strong scaling behavior all the way to 30B parameters, achieving competitive performance across a wide range of benchmarks.

Building performant MLLMs is a highly empirical endeavor. While the overarching goal and the high-level training procedure are well-defined, the finer details of their execution remain unclear. In developing MM1.5, we choose to retain the same model architecture as MM1 (McKinzie et al., 2024), enabling us to focus on refining and investigating the intricacies of our data-centric training recipes. Our attention is centered on the following key aspects:

- **Continual Pre-training.** We introduce an additional high-resolution continual pre-training stage preceding the SFT stage, which we found crucial for boosting text-rich image understanding performance. We ablate the impact of two kinds of data: (i) text-rich OCR data, focusing on detailed transcription of text within images; and (ii) high-quality synthetic image captions.
- **SFT.** While considerable prior work discusses SFT data for MLLMs, there is still limited exploration into how each category of SFT data can affect the final model’s performance. In particular, the impact of data supporting each capability on other capabilities is understudied. We conduct extensive ablations to identify trade-offs and synergies, ultimately constructing a mixture from public datasets that contributes to well-balanced performance across a wide set of capabilities.
- **Dynamic High-resolution.** Furthermore, for *high-resolution* image encoding, we follow the popular any-resolution approach, dynamically dividing the image into sub-images (Li et al., 2023i; Zhang et al., 2024b), and conduct thorough ablations to refine key details in our design.

Unlike most open-source models focusing solely on SFT (Liu et al., 2023b;a; 2024a), MM1 demonstrated strong zero-shot and few-shot learning capabilities through large-scale pre-training. In developing MM1.5, we aim to retain these strengths and more effectively transfer them to the SFT stage. To achieve this, We further extend MM1’s pre-training by exploring the impact of text-only data and optimizing the ratio of different pre-training data types. This approach improves performance on knowledge-intensive benchmarks and enhances overall multimodal understanding capabilities.

Our main contributions are summarized as follows: (i) We introduce MM1.5, a family of MLLMs that include both dense models (ranging from 1B to 30B) and MoE variants. (ii) We conduct a thorough empirical study detailing the process and decisions leading to our final design choices. (iii) MM1.5 excels in handling a wide range of multimodal tasks, from general-domain to text-rich image understanding, coarse- to fine-grained understanding, and single- to multi-image reasoning.

2 RECIPE FOR BUILDING MM1.5

In this work, beyond pre-training and SFT stages as in MM1 (McKinzie et al., 2024), we introduce a continual pre-training stage with high-quality OCR data and synthetic captions. As outlined in Figure 1, to obtain the best data recipe,

- We first present comprehensive ablations of our SFT data mixture (Section 2.2). We categorize the SFT data into multiple groups based on the capabilities they aim to support. We carefully evaluate the impact of datasets from each category and adjust the ratio to balance different core capabilities.

- To further enhance model performance, especially for text-rich image understanding, we further ablate the data choices for continual pre-training (Section 2.3). This includes 45M rich OCR data and 7M high-quality captions from public or generated by a MM1-based image captioner.
- We also provide detailed ablation regarding dynamic image splitting, also known as AnyRes (Liu et al., 2024a) (Section 2.4), for high-resolution image comprehension.

Finally, to enhance performance on knowledge-heavy benchmarks like MMMU (Yue et al., 2023a), we further study the impact of pre-training data (Appendix A.2).

2.1 EMPIRICAL SETUP FOR ABLATIONS

Unless otherwise noted, we follow the default settings below in our ablation studies.

Model architecture and data preprocessing. We follow MM1 (McKinzie et al., 2024) and use the same architecture, focusing on the 3B dense model for all the ablation studies in this section. Specifically,

- Static image splitting (Lin et al., 2023b) is enabled with 4 sub-image splits (plus an overview image), and each sub-image is resized to 672×672 resolution via position embedding interpolation. Note that we did not use dynamic image splitting during ablation for faster iteration of experiments.
- As to the encoding of multi-image data, we enable image splitting only when the current training sample contains fewer than three images to avoid excessively long sequence lengths.
- Similar to capabilities introduced in Ferret (You et al., 2023), MM1.5 directly supports referring and grounding. When requested, MM1.5 can produce bounding boxes in its textual output to ground its responses. Additionally, the model can interpret references to points and regions in the input image in the form of referring coordinates and bounding boxes.
- The CLIP image encoder and the LLM backbone are based on in-house models, with C-Abstractor (Cha et al., 2024) serving as the vision-language connector.

Model optimization. For both continual pre-training and SFT, we set the batch size as 256. We use the AdaFactor optimizer with a peak learning rate of $1e-5$ and a cosine decay of 0. For continual pre-training, we train a maximum of 30k steps. During SFT, all models are optimized for one epoch.

Continual pre-training. Models are initialized with the MM1 pre-trained checkpoint. By default, we conduct continual pre-training on 45M high-resolution OCR data (including PDFFA, IDL, Rendered-text (Laureçon et al., 2024a) and DocStruct-4M (Hu et al., 2024a)) at this stage. In each training batch, data is equally sampled from those four datasets. Similar to the SFT stage, we use static image splitting, dividing each image into five sub-images, with each sub-image resized to 672×672 resolution. We find that this high-resolution setup is essential for continual pre-training.

SFT data categorization. Grouping datasets into categories can be helpful for data balancing and simplifying the analysis (Laureçon et al., 2024a; Tong et al., 2024a). At a high level, we cluster datasets into *single-image*, *multi-image*, and *text-only* categories based on the number of images presented in each example. For the single-image group, we further classify each dataset into the following sub-categories: *general*, *text-rich*, *refer&ground*, *science*, *math* and *code*. See Table 5 in Appendix A.3 for the details of each category used for the ablation study, and Figure 8 for an overview of the group categories.

Evaluation benchmarks. We group our benchmarks into categories based on what capabilities a benchmark primarily measures. Our benchmark groups include general, text-rich, refer&ground, knowledge, and multi-image. See Table 6 in Appendix A.4 for more details. We propose *Category Average Score*, the average score of all benchmark numbers for each sub-category, to represent the average performance on that capability. We focus on the categories of general, text-rich, and knowledge, as these capabilities are widely considered essential for MLLMs. To evaluate a model’s impact on these capabilities, we refer to a *MMBase* score, defined as the average scores on general, text-rich, and knowledge categories. Details of the evaluation metrics are provided in Appendix A.4.

2.2 SFT ABLATIONS

To determine the optimal SFT recipe, we first study the impact of different data categories in Section 2.2.1, followed by investigating how to best mix all the data in Section 2.2.2.

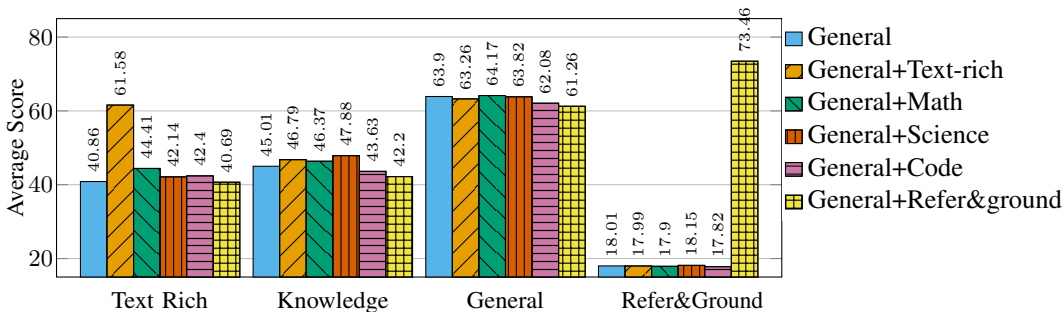


Figure 2: Impact of different SFT data categories to different model capabilities (general, text-rich, knowledge, and refer&ground). Text-rich data significantly improves text-rich and knowledge benchmarks on average. Science data improves knowledge average score. Referring and grounding data enables this capability.

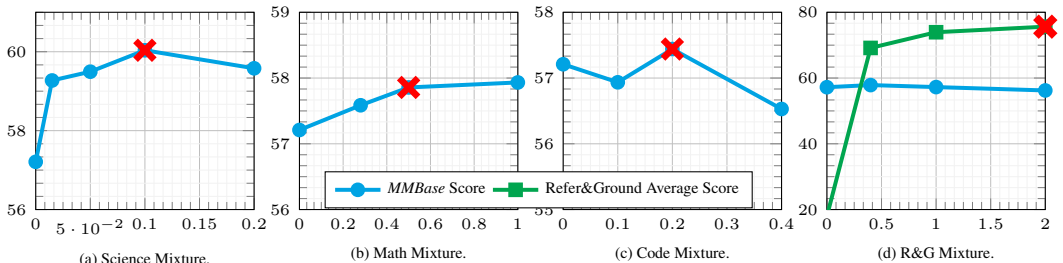


Figure 3: Impact of α (x -axis) for different data categories to a model’s different capabilities. The selected ratio is marked with red “x”. α denotes the data ratio of the target category (science, math, code, refer&ground (R&G)) when compared with the general category.

2.2.1 IMPACT OF DIFFERENT DATA CATEGORIES

In this subsection, we focus on evaluating the single-image data category. We begin by assessing the general data category and then progressively evaluate the impact of adding other sub-categories individually. During training, we mix data from different sub-categories and construct each training batch by randomly sampling data from the corresponding mixture. We compare models using each capability with the *Category Average Score*.

Our results are summarized in Figure 2. We observe that adding text-rich data can significantly improve the performance on text-rich and knowledge benchmarks. The inclusion of math data follows a similar trend, though we observe a lesser degree of improvement in the text-rich average score. When science data is added, we observe the expected improvement in the knowledge benchmarks, alongside a minor improvement in text-rich performance. Adding the code category yields a slight increase in the text-rich average score, while the performance on other benchmarks does not improve. Including the refer&ground data instills the model with referring and grounding capability, but we also observe slight regression in all other capability categories.

2.2.2 DATA MIXTURE RATIO STUDY

We first study the mixing ratio within the single-image categories. Since directly mixing the general and text-rich data based on their data sizes shows strong results across a variety of benchmarks (see Figure 2), we use this combination as the starting point to study how to mix other categories to this set. Then, we combine the entire single-image set with multi-image and text-only sets with sampling weights of w_{single} , w_{multi} and w_{text} , respectively, where $w_{\text{single}} + w_{\text{multi}} + w_{\text{text}} = 1$.

Mixture of single-image data. Directly mixing all datasets from different categories may not be ideal due to imbalanced numbers of data samples across different sub-categories. For example, the size of the general data category is around $68\times$ the size of the science data category. In this study, we use the general data category as the reference, and upsample/downsample data from a target category, such that in each training batch, the data ratio from the general and target category is $1:\alpha$.

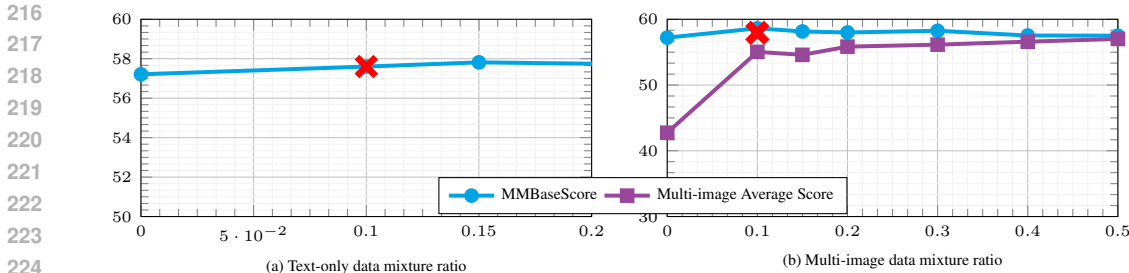


Figure 4: Impact of the mixing ratio for text-only and multi-image SFT data. The selected ratio is marked with red “x”.

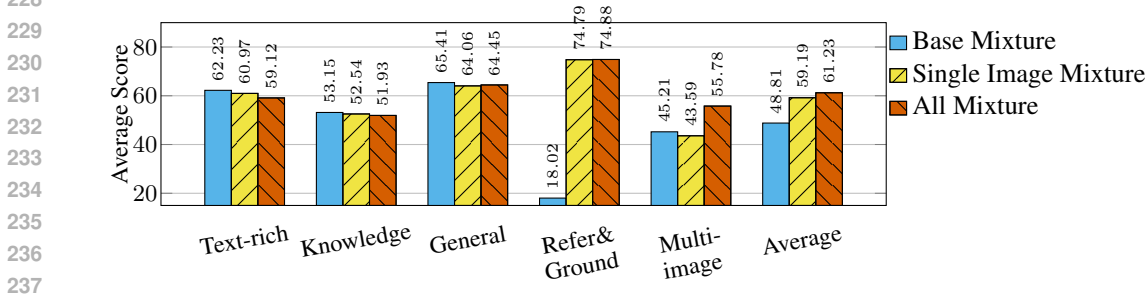


Figure 5: Ablation study of mixing all the SFT data. *Base Mixture* denotes general, text-rich and knowledge (science, math and code). The “Average” column represents the performance averaged across the preceding five benchmark categories.

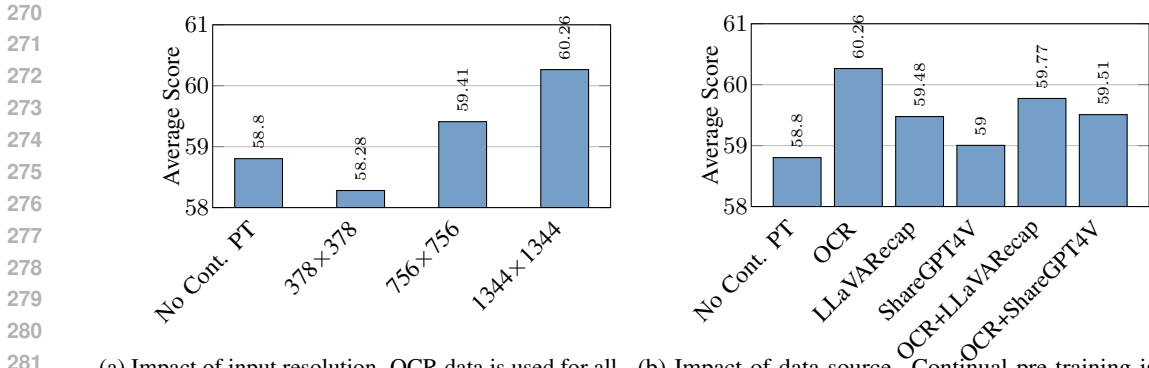
To measure the average impact of α , we propose *MMBase* score, an average over general, text-rich, and knowledge average scores, for model comparison. As shown in Figure 3, we vary the α for different data categories. For science, math, and code categories, we find the best ratio of α to be 0.1, 0.5, and 0.2, respectively. As shown in Section 2.2.1, the refer&ground data is the main driver for improving referring and grounding benchmarks. Therefore, besides the *MMBase* score, we also include the Refer&Ground average score as another metric for the α selection. As summarized in Figure 3(d), the *MMBase* score will drop slightly, while the Refer&Ground average score increases significantly. With that, we select $\alpha = 2.0$ as a good trade-off.

Mixture of single-image, multi-image, and text-only data. Now, we study the mixture ratios, w_{single} , w_{multi} and w_{text} . Enumerating all combinations between the three ratios will incur significant computational cost. Therefore, we instead separately ablate w_{text} and w_{multi} for text-only and multi-image data, respectively, to evaluate how sensitive our model is to these ratios. Finally, w_{single} is determined by $1 - w_{\text{text}} - w_{\text{multi}}$.

Similar to the single-image mixture study, we also start with the combination of general and text-rich data and enumerate different values for w_{multi} and w_{text} . For text-only data, we tested w_{text} from 0 to 0.2. Figure 4(left) shows that varying different values for w_{text} has minor effects on the model’s base capabilities in general. We select $w_{\text{text}} = 0.1$ to allocate a higher weight for single-image data for potential performance improvements.

For multi-image data, we use the multi-image average score (evaluated on multi-image benchmarks in Table 6) as an additional metric to assess a model’s capability of handling multi-image tasks. Results are summarized in Figure 4(right). We observe that increasing the sampling ratio of multi-image data would introduce a performance drop of the base capabilities as indicated by the decreased number of the *MMBase* score, while the multi-image average score increases. We select $w_{\text{multi}} = 0.1$ since it introduces a surge in the multi-image average score.

Mixing multiple categories. Based on the studies above, we present three mixtures, the *Base* mixture, *Single-image* mixture, and *All* mixture, and analyze their trade-offs. The *Base* mixture includes the general, text-rich, science ($\alpha_{\text{science}} = 0.1$), math ($\alpha_{\text{math}} = 0.5$) and code ($\alpha_{\text{code}} = 0.2$) data groups. The *Single-image* mixture additionally adds refer&ground data ($\alpha_{\text{rg}} = 2.0$) to the *Base* mixture. *All*



(a) Impact of input resolution. OCR data is used for all the continual pre-training experiments.

(b) Impact of data source. Continual pre-training is conducted in the high-resolution (1344×1344) setting.

Figure 6: Ablation study of continual pre-training. Average Score indicates the *MMBase* score. Cont. PT denotes continual pre-training.

mixture includes all data from single-image, multi-image, and text-only data, with $w_{\text{single}} = 0.8$, $w_{\text{multi}} = 0.1$, and $w_{\text{text}} = 0.1$.

Our results are summarized in Figure 5. The first three columns indicate that including refer&ground and multi-image data slightly reduces average performance on text-rich, knowledge, and general benchmarks. The fourth column shows that adding refer&ground data significantly boosts referring and grounding performance, while the fifth column highlights that adding multi-image data greatly improves multi-image benchmarks. The final column reveals that our optimized mixture achieves the best overall performance, balancing all capabilities across benchmarks.

2.3 CONTINUAL PRE-TRAINING ABLATIONS

Unless otherwise specified, we use OCR data (45M in total), including PDFa, IDL, Rendered-text (Laureçon et al., 2024a) and DocStruct-4M (Hu et al., 2024a) in a high-resolution setting (1344×1344) for continual pre-training. During the SFT stage, all continual pre-trained models in this section are fine-tuned with data from the *Base Mixture* including general, text-rich, knowledge (science, math, and code) with their selected mixture ratios as described in Section 2.2.2.

Impact of image resolution. Intuitively, higher-resolution images are preferable when training with OCR data. We first ablate the impact of image resolution during this stage by setting up two baselines, continual pre-training with 378×378 and 756×756 resolutions, respectively. For the former, we disabled both image splitting and position embedding interpolation (our CLIP image encoder natively supports image resolution of 378×378). For the latter, we enabled image splitting and turn-off position embedding interpolation. The results are shown in Figure 6(a). Note that the final SFT stage always uses image resolution 1344×1344 across these experiments, so the training only differs with respect to the image resolution used in continual pre-training.

We can clearly see that using a setting of 1344×1344 image resolution for continual pre-training achieves the best overall performance. Decreasing resolution consistently leads to lower final scores. In particular, continual pre-training with 378×378 resolution can underperform a model without continual pre-training. We hypothesize this is due to insufficient visible detail at lower resolutions, which may hinder the model’s ability to effectively learn from the document-based OCR data in the continual pre-training mixture.

Impact of OCR data and synthetic captions. Besides OCR data, high-quality synthetic image captions (Chen et al., 2023c; Li et al., 2024a) are also widely considered useful for pre-training. To study its impact, we use our default setting except for the data used in continual pre-training. We study two synthetic caption datasets: LLaVA-Recap-3M (Li et al., 2024a) and ShareGPT4V-PT (Chen et al., 2023c), and their combination with our OCR data. When we combine ShareGPT4V-PT or LLaVA-Recap-3M with our OCR data, we equally sample data from individual datasets in each training batch. Results are presented in Figure 6(b). We observe that all continual pre-trained models perform better than the baseline without continual pre-training. However, we did not find conclusive evidence that these high-quality synthetic captions improved performance over the arguably simpler

Table 1: Ablation on the image resolution and the number of image tokens used in dynamic image splitting. n denotes the total number of sub-images. Row 3: $(n_{\min}, n_{\max}) = (4, 4)$; Row 4-7: $(n_{\min}, n_{\max}) = (9, 9)$. Image encoder resolution: (i) 378×378 : no position embedding interpolation; (ii) 672×672 : with position embedding interpolation.

Row #	Mode	n	#image tokens (per sub-img / total)	Image Enc. Resolution	Effective Resolution	Text-rich	Knowledge	General	Refer & Ground	Average
1	Static	1	144/144	672×672	0.45MP	49.4	53.6	62.6	71.3	59.2
2		5	144/720	672×672	1.8MP	57.7	53.8	64.4	74.8	62.7
3	Dynamic	5	144/720	672×672	1.8MP	58.6	53.7	64.1	74.0	62.5
4		10	81/810	378×378	1.3MP	57.6	53.3	62.9	74.0	62.0
5		10	81/810	672×672	4.1MP	58.3	53.8	64.3	74.9	62.8
6		10	144/1440	378×378	1.3MP	58.5	54.0	63.2	74.5	62.6
7		10	144/1440	672×672	4.1MP	59.8	54.0	64.5	75.2	63.3

OCR data. While prior studies (Li et al., 2024c) show synthetic captions boost performance, our results indicate further investigation into their exact impact is needed.

Therefore, we further investigate the impact of synthetic captions generated through self-training for even larger scales (up to 7M) and more controllable styles, using a pre-trained MM1 model fine-tuned on human-annotated captions, similar to (Fang et al., 2024). This new dataset showed some promise in certain settings, see Appendix A.5 for details. We defer further study of this topic to future work.

2.4 DYNAMIC IMAGE SPLITTING ABLATIONS

Dynamic image splitting. Processing high-resolution images is essential for text-rich image understanding. In *static* image splitting (Lin et al., 2023b), images are split into a rigid 2×2 grid, which is often inefficient. Low-resolution images are splitted without any need, and images with non-square aspect ratios can result in sub-images being padding only. Therefore, we adopt a dynamic image splitting approach, which is common in the literature (Li et al., 2024a; Dong et al., 2024b; Hu et al., 2024a; Lin et al., 2023b; Xu et al., 2024c; Zhang et al., 2024d), for MM1.5.

Given a minimum and maximum number of sub-images, n_{\min} and n_{\max} , consider the set of all candidate grids $G = \{(n_h, n_w) \in \mathbb{N} \mid n_{\min} \leq n_h \cdot n_w \leq n_{\max}\}$. Further, consider the resolution of the vision encoder r , and an input image resolution (h, w) . If there is a grid that can cover the image, we choose the grid that minimizes the amount of padding after longer side resizing to the grid, *i.e.*, $g^* = \arg \min_{(n_h, n_w) \in G} n_h n_w r^2 - h_g w_g$, subject to $n_h r \geq h_g \geq h$ and $n_w r \geq w_g \geq w$, where h_g, w_g denote the image height and width after longer side resizing the candidate grid. If no such grid exists, we choose the one that minimizes the resolution loss due to scaling the image down and fully covers the longer side resized image. Assume we allow up to 4 sub-images. With a static image splitting approach, all images use the grid (2, 2). The dynamic splitting approach instead allows for the following grids: $\{(1, 1), (1, 2), (2, 1), (1, 3), (3, 1), (1, 4), (4, 1), (2, 2)\}$.

Global-Local Format. In addition to the sub-images, we always feed the original image with a longer side resized to the encoder resolution r to the model. This ensures that the model has a global understanding of the image. If the grid is (1, 1), we omit the overview image. We consider two variants: (i) **before**: the overview image is put before the sub-images; (ii) **after**: the overview image is put after the sub-images. These variants yield different results because an autoregressive mask is used in the LLM decoder, and as such, the choice determines whether the decoder can attend to the overview image when processing the sub-images (i) or attend to the sub-images when processing the overview image (ii).

Sub-image position indicator. Given that an input image is dynamically split into multiple sub-images, we explore whether it is helpful to indicate the position of each sub-image in the original high-resolution image to ensure the model can understand the original 2D image structure. Specifically, we consider two methods.

- **Index.** A tuple of (k, i, j) is used to represent sub-image position information, where k is the zero-indexed image number in the example (assuming there can be multiple images in a training sample), i and j are the one-index row and column id, *e.g.*, $(0, 0, 0)$ is the overview image of image 0, and $(0, 2, 1)$ is the sub-image in the second row and first column, for image 0.

Table 2: Ablation on the image grid configuration (n_{\min}, n_{\max}) used in dynamic image splitting.

Row #	(n_{\min}, n_{\max})		DocVQA	InfoVQA	Text-rich	Knowledge	General	Refer & Ground	Average
	Train	Inference							
<i>3B Model Comparison</i>									
1	(4, 4)	(4, 4)	73.2	48.3	58.6	53.3	64.1	74.0	62.5
2	(4, 9)	(4, 9)	75.7	53.8	60.0	54.0	63.9	74.6	63.1
3	(4, 16)	(4, 16)	76.3	55.2	60.7	53.4	64.0	73.8	63.0
4	(1, 9)	(1, 9)	76.2	54.1	60.4	53.7	62.5	71.5	62.0
5	(4, 4)	(4, 9)	73.4	52.9	59.7	53.5	63.8	74.0	62.8
6	(4, 4)	(4, 16)	72.3	53.5	59.6	53.8	63.5	74.0	62.7
7	(4, 4)	(1, 9)	73.5	52.7	59.8	50.7	62.6	24.5	49.4
<i>7B Model Comparison</i>									
8	(4, 4)	(4, 4)	77.0	54.3	64.5	61.1	66.8	77.7	67.5
9	(4, 9)	(4, 9)	81.7	62.1	67.4	60.1	66.6	78.0	68.0
10	(4, 16)	(4, 16)	83.3	64.1	68.0	58.7	67.7	77.2	67.9

Table 3: Ablation on the sub-image position indicator and the position of the overview image. We set $(n_{\min}, n_{\max}) = (4, 4)$ for experiments.

Row #	Sub-img pos. indicator	Overview image pos.	DocVQA	InfoVQA	Text-rich	Knowledge	General	Refer & Ground	Average
1	none	before	73.2	48.3	58.6	53.5	64.1	74.0	62.5
2	seps	before	74.3	49.7	58.8	53.0	63.8	74.5	62.5
3	index	before	73.4	48.6	58.6	52.7	63.4	74.8	62.4
4	none	after	73.3	49.7	59.2	54.3	64.1	73.8	62.8

• **Septs.** Instead of using indexes, we use three text tokens. Specifically, ‘:’ is the overview image indicator, ‘,’ is the column separator, and ‘<n>’ is the row separator. The latter two tokens are inserted between the set of image tokens corresponding to each sub-image so that the original 2D image structure can be recovered from the flattened image token sequence.

Inference for higher resolution. The tuple (n_{\min}, n_{\max}) is used to decide the dynamic image splitting configuration for model training. During inference, it is possible to support even higher-resolution image processing simply by increasing these parameters. For example, we explore training at $(n_{\min}, n_{\max}) = (4, 9)$ to save model training compute, while during inference, we use $(n'_{\min}, n'_{\max}) = (4, 16)$ to process images at even higher effective resolutions.

Findings. We use the final *Single-image Mixture* as our default experiment setting, including general, text-rich, knowledge (science, math and code), and refer&ground data. For fast iteration of experiments, all the models are initialized with the MM1 pre-trained checkpoint without continual pre-training. Following Figure 2, we report the average performance on text-rich, knowledge, general, and refer&ground benchmarks. Our findings are summarized as follows.

- Dynamic image splitting outperforms static splitting in text-rich tasks. Both image resolution and the number of sub-images, along with image token counts, are important (Table 1).
- Regarding image grid configuration (Table 2), dynamic image splitting with a larger n_{\max} significantly improves performance on tasks with unusual aspect ratios, such as DocVQA and InfoVQA, especially when trained natively for it. Grounding performance is highly sensitive to grid size changes, and larger LLM backbones yield greater performance gains, with the 7B model showing larger improvements than the 3B model.
- In terms of position indicators (Table 3), they are not strictly necessary for text-rich tasks, though they can be beneficial for specific tasks like DocVQA and InfoVQA. Additionally, placing the overview image after the sub-images improves performance, as it allows the decoder attention mask to attend to all sub-images more effectively.
- In practice, dynamic image splitting does not significantly increase the number of sub-images to process. In a sample of 100k examples, static splitting generates 500k sub-images, while dynamic splitting with $(n_{\min}, n_{\max}) = (4, 9)$ produces barely more, only 539k images in total.

3 FINAL MODEL AND TRAINING RECIPE

We collect the results from the previous ablations to determine the final recipe for MM1.5 training:

- **Architecture.** We use the same model architecture as MM1 (McKinzie et al., 2024).
- **Data and training pipeline.** As summarized in Figure 1, MM1.5 is trained in three stages:
 - **Pre-training.** The pre-training data comprises three parts: (i) 2B image-text pairs, (ii) 600M interleaved image-text documents with 1B images in total, and (iii) text-only data with 2T tokens. Except for the updated text-only data, the data remains unchanged from MM1 (McKinzie et al., 2024). However, the data ratio has been adjusted from 45:45:10 to 50:10:40, significantly downweighting the interleaved data (from 45% to 10%) while increasing the proportion of text-only data (from 10% to 40%) as discussed in Section A.2.
 - **Continual Pre-training.** We use 45M OCR data to enhance text-rich image understanding. Notably, we do not include additional synthetic image captions based on empirical results.
 - **SFT.** We use the data illustrated in Figure 8 and adopt the mixing ratios studied in Section 2.2.2. Our final mixture consists of 80% single-image data, 10% multi-image data, and 10% text-only SFT data. The single-image data can be further categorized into 37.2% text-rich data, 22.5% refer&ground data (VQA data enriched with bounding boxes and/or point coordinates), 11.3% general data, 5.6% math data, 2.3% code data, and 1.1% science data, totaling 80% of all data.
- **Dynamic high-resolution.** We set the image grid configuration $(n_{\min}, n_{\max}) = (4, 9)$, using an index for the sub-image position indicator and placing the overview image after the sub-images. Dynamic image splitting is only enabled when the current training sample has fewer than three images. The supported resolution reaches up to 4 Megapixels (approximately 2016×2016 for a square image, or 6048×672 for a long image).

We use the same image encoder and the LLM backbone from MM1 (McKinzie et al., 2024), and keep them *unfrozen* during all the model training stages. For pre-training, we follow the exact same learning rate schedule as in MM1 (McKinzie et al., 2024) and 200k training steps with sequence length 4096. For continual pre-training, we use a peak learning rate of $1e-5$ with the cosine decay and 30k training steps for all the models (from 1B to 30B). For SFT, we use a peak learning rate of $2e-5$ and 23k training steps for all the models.²

Mixture-of-Experts (MoE). We introduce two MoE models, a 1B-MoE and a 3B-MoE, with 64 experts replacing dense layers every two layers. We use the same hyperparameters as those applied to the dense models for both scales and top-2 gating with a 0.01 load balance loss to encourage a better expert load balance and a 0.001 router z-loss for training stability (Lepikhin et al., 2021).

3.1 RESULTS

We evaluate our MM1.5 models across 35 multimodal benchmarks using an internal fork of lm-eval-harness (Gao et al., 2023), covering task categories ranging from general multimodal understanding, knowledge, text-rich, referring and grounding, multi-image reasoning, to in-context learning. Detailed results for each capability at various model sizes are further summarized in Table 7, 8, 9, 10, and 11, respectively. Below, we highlight a few key observations from Table 4.

MM1.5 represents a major upgrade over MM1. It delivers improvements across all model sizes and nearly all benchmarks, often by a substantial margin. For instance, MM1.5-30B boosts the MathVista from 39.4 to 55.6, DocVQA from 75.8 to 91.4, and InfoVQA from 47.3 to 67.3. It also offers much enhanced multi-image reasoning capability and introduces new capabilities not present in MM1, such as visual referring & grounding.

Both Dense and MoE model scaling are effective. First, scaling the dense model from 1B to 30B consistently improves performance, with benchmarks like AI2D increasing from 59.3 to 77.2 (see Table 7). Second, both the 1B and 3B MoE models outperform their dense counterparts. Notably, the MM1.5-3B-MoE model can even surpass the MM1.5-7B model in knowledge, general, visual referring and grounding, and multi-image benchmarks, though it falls slightly behind on text-rich benchmarks. This suggests that MoE models show strong potential in integrating diverse capabilities compared to dense models.

²All models are trained using the AXLearn framework <https://github.com/apple/axlearn>

Table 4: Comparison with SOTA models on the selected benchmarks. Comparison of more benchmarks and broader baselines can be found in Table 7,8,9, 10 and 11 in the Appendix.

Model	Text-rich			Knowledge		General		Refer&Ground		Multi-image	In-context
	TextVQA (val)	DocVQA (test)	InfoVQA (test)	MMMU (val)	MathV (testmini)	SEED ¹	RealWorldQA	RefCOCO avg	LVIS avg	NLVR2 (val)	VL-ICL avg
<i>1B Model Comparison</i>											
LLaVAVision-0.5B	–	70.0	41.8	31.4	34.8	65.5	55.6	–	–	63.4	–
SPHINX-Tiny	57.8	53.0	26.3	–	26.4	–	–	77.2	–	–	–
MM1-1B	68.2	68.4	38.5	33.2	31.1	65.6	51.2	–	51.5	50.9	34.3
MM1.5-1B	72.5	81.0	50.5	35.8	37.2	70.2	53.3	81.4	62.2	79.0	51.0
MM1.5-1B-MoE	76.1	84.8	55.9	41.2	42.9	71.4	57.8	83.9	64.1	83.2	56.0
<i>3B Model Comparison</i>											
IntenVL2-2B	73.4	86.9	58.9	36.3	46.0	70.9	57.4	77.7	51.1	67.4	18.5
MiniCPM-V 2.0-3B	74.1	71.9	37.6	38.2	38.7	67.1	55.8	–	48.0	–	–
Phi-3-Vision-4B	70.1	83.3	49.0	40.4	44.5	71.8	59.4	38.1	54.2	53.6	19.5
MM1-3B	71.9	75.2	44.7	33.9	32.0	68.8	55.8	–	53.4	51.7	37.0
MM1.5-3B	76.5	87.7	58.5	37.1	44.4	72.4	56.9	85.6	67.9	83.8	56.3
MM1.5-3B-MoE	76.8	85.0	53.6	42.9	46.9	73.3	60.7	86.2	66.9	86.0	59.6
<i>7B Model Comparison</i>											
MM1-7B	72.8	76.8	45.5	37.0	35.9	69.9	55.7	–	53.2	59.9	52.8
MM1.5-7B	76.5	88.1	59.5	41.8	47.6	73.4	62.5	86.6	66.4	86.9	56.0
<i>30B Model Comparison</i>											
MM1-30B	73.5	75.8	47.3	44.7	39.4	72.1	59.4	–	53.1	63.1	52.1
MM1.5-30B	79.2	91.4	67.3	47.4	55.6	75.0	69.0	90.1	73.2	90.6	77.6

MM1.5-1B is the state-of-the-art model at the 1B scale. While few models are available at this scale, MM1.5-1B clearly outperforms comparable models such as SPHINX-Tiny (Gao et al., 2024). For reference, MM1.5-1B also significantly surpasses LLaVAVision-0.5B (Li et al., 2024c) (e.g., ScienceQA: 67.2 vs. 82.1, DocVQA: 70.0 vs. 81.0, see Table 7 and 8), but it should be stressed that this is of course an even smaller model and as such cannot be directly compared.

MM1.5-3B outperforms MiniCPM-V 2.0 and is competitive with InternVL2 and Phi-3-Vision. Compared to MiniCPM-V 2.0, MM1.5-3B achieves superior results on MathVista (38.7 vs. 44.4) and DocVQA (71.9 vs. 87.7) while also supporting visual referring and grounding, which MiniCPM-V lacks. It surpasses InternVL2-2B on general VQA and, although Phi-3-Vision (4.2B) has an edge on knowledge-based tasks like AI2D as in Table 7, MM1.5-3B excels on text-rich benchmarks (e.g., DocVQA: 83.3 vs. 87.7) and outperforms Phi-3-Vision in referring and grounding (see Table 9), as well as in-context learning tasks (see Table 10).

MM1.5 excels in visual referring and grounding. While most SOTA models focus on improving performance across general, knowledge, and text-rich benchmarks, few have integrated fine-grained image grounding and referring ability into their design. Even GPT-4o relies on set-of-mark prompting to demonstrate visual grounding capabilities. As shown in Table 9, MM1.5-3B outperforms Ferret-7B and is on par with Ferret-13B, both of which are fine-tuned specifically for referring and grounding tasks. Notably, our model inherently possesses these capabilities while still excelling in other areas.

MM1.5 excels in multi-image reasoning and in-context learning. As shown in Table 11, the MM1.5-1B model outperforms LLaVAVision-0.5B at the 1B scale. Similarly, at the 3B scale, MM1.5-3B significantly surpasses Phi-3-Vision. Additionally, we evaluate MM1.5’s zero-shot transfer capability for video understanding using MVBench (Li et al., 2024h), a benchmark designed for video tasks. Moreover, we evaluate MM1.5’s ability of multimodal in-context learning on VL-ICL benchmark (Zong et al., 2024). As shown in Table 10, our models outperform others in in-context learning. In Section A.7, we will further introduce MM1.5-Video, a model variant specifically designed for video understanding.

4 CONCLUSION AND LIMITATION

In this work, we build on the insights of MM1 (McKinzie et al., 2024) and introduce MM1.5, a family of highly performant generalist MLLMs. While MM1 focused on key pre-training choices, we improve post-pre-training techniques like continual pre-training, dynamic high-resolution image processing, and curation of our supervised fine-tuning datasets. Our extensive ablations show MM1.5’s strong performance in text-rich image understanding, visual grounding, and multi-image reasoning. Like most MLLMs, MM1.5 may produce harmful and counterfactual responses. Future efforts will aim to unify these capabilities for a stronger generalist model, with the hope of benefiting the community beyond specific architectures.

REFERENCES

- wendlerc/renderedtext.
- Marah Abdin, Sam Ade Jacobs, Ammar Ahmad Awan, Jyoti Aneja, Ahmed Awadallah, Hany Awadalla, Nguyen Bach, Amit Bahree, Arash Bakhtiari, Jianmin Bao, Harkirat Behl, Alon Benhaim, Misha Bilenko, Johan Bjorck, Sébastien Bubeck, Qin Cai, Martin Cai, Caio César Teodoro Mendes, Weizhu Chen, Vishrav Chaudhary, Dong Chen, Dongdong Chen, Yen-Chun Chen, Yi-Ling Chen, Parul Chopra, Xiyang Dai, Allie Del Giorno, Gustavo de Rosa, Matthew Dixon, Ronen Eldan, Victor Fragoso, Dan Iter, Mei Gao, Min Gao, Jianfeng Gao, Amit Garg, Abhishek Goswami, Suriya Gunasekar, Emman Haider, Junheng Hao, Russell J. Hewett, Jamie Huynh, Mojan Javaheripi, Xin Jin, Piero Kauffmann, Nikos Karampatziakis, Dongwoo Kim, Mahoud Khademi, Lev Kurilenko, James R. Lee, Yin Tat Lee, Yuanzhi Li, Yunsheng Li, Chen Liang, Lars Liden, Ce Liu, Mengchen Liu, Weishung Liu, Eric Lin, Zeqi Lin, Chong Luo, Piyush Madan, Matt Mazzola, Arindam Mitra, Hardik Modi, Anh Nguyen, Brandon Norick, Barun Patra, Daniel Perez-Becker, Thomas Portet, Reid Pryzant, Heyang Qin, Marko Radmilac, Corby Rosset, Sambudha Roy, Olatunji Ruwase, Olli Saarikivi, Amin Saied, Adil Salim, Michael Santacrose, Shital Shah, Ning Shang, Hiteshi Sharma, Swadheen Shukla, Xia Song, Masahiro Tanaka, Andrea Tupini, Xin Wang, Lijuan Wang, Chunyu Wang, Yu Wang, Rachel Ward, Guanhua Wang, Philipp Witte, Haiping Wu, Michael Wyatt, Bin Xiao, Can Xu, Jiahang Xu, Weijian Xu, Sonali Yadav, Fan Yang, Jianwei Yang, Ziyi Yang, Yifan Yang, Donghan Yu, Lu Yuan, Chengruidong Zhang, Cyril Zhang, Jianwen Zhang, Li Lyna Zhang, Yi Zhang, Yue Zhang, Yunan Zhang, and Xiren Zhou. Phi-3 technical report: A highly capable language model locally on your phone, 2024a.
- Marah Abdin, Sam Ade Jacobs, Ammar Ahmad Awan, Jyoti Aneja, Ahmed Awadallah, Hany Awadalla, Nguyen Bach, Amit Bahree, Arash Bakhtiari, Harkirat Behl, et al. Phi-3 technical report: A highly capable language model locally on your phone. *arXiv preprint arXiv:2404.14219*, 2024b.
- Jean-Baptiste Alayrac, Jeff Donahue, Pauline Luc, Antoine Miech, Iain Barr, Yana Hasson, Karel Lenc, Arthur Mensch, Katherine Millican, Malcolm Reynolds, et al. Flamingo: a visual language model for few-shot learning. *NeurIPS*, 2022.
- Anthropic. Claude 3 model card, 2023. URL https://www-cdn.anthropic.com/de8ba9b01c9ab7cbabf5c33b80b7bbc618857627/Model_Card_Claude_3.pdf. Accessed: 2024-08-13.
- Anas Awadalla, Irena Gao, Josh Gardner, Jack Hessel, Yusuf Hanafy, Wanrong Zhu, Kalyani Marathe, Yonatan Bitton, Samir Gadre, Shiori Sagawa, et al. Openflamingo: An open-source framework for training large autoregressive vision-language models. *arXiv preprint arXiv:2308.01390*, 2023.
- Anas Awadalla, Le Xue, Oscar Lo, Manli Shu, Hannah Lee, Etash Kumar Guha, Matt Jordan, Sheng Shen, Mohamed Awadalla, Silvio Savarese, et al. Mint-1t: Scaling open-source multimodal data by 10x: A multimodal dataset with one trillion tokens. *arXiv preprint arXiv:2406.11271*, 2024.
- Gilles Baechler, Srinivas Sunkara, Maria Wang, Fedir Zubach, Hassan Mansoor, Vincent Etter, Victor Carbune, Jason Lin, Jindong Chen, and Abhanshu Sharma. Screenai: A vision-language model for ui and infographics understanding. In *IJCAI*, 2024.
- Jinze Bai, Shuai Bai, Shusheng Yang, Shijie Wang, Sinan Tan, Peng Wang, Junyang Lin, Chang Zhou, and Jingren Zhou. Qwen-vl: A frontier large vision-language model with versatile abilities. *arXiv preprint arXiv:2308.12966*, 2023.
- Jonas Belouadi, Anne Lauscher, and Steffen Eger. Automatizk: Text-guided synthesis of scientific vector graphics with tikz. *arXiv preprint arXiv:2310.00367*, 2023.
- Lucas Beyer, Andreas Steiner, André Susano Pinto, Alexander Kolesnikov, Xiao Wang, Daniel Salz, Maxim Neumann, Ibrahim Alabdulmohsin, Michael Tschannen, Emanuele Bugliarello, et al. Paligemma: A versatile 3b vlm for transfer. *arXiv preprint arXiv:2407.07726*, 2024.
- Ali Furkan Biten, Ruben Tito, Andres Mafla, Lluís Gomez, Marçal Rusinol, Ernest Valveny, CV Jawahar, and Dimosthenis Karatzas. Scene text visual question answering. In *ICCV*, 2019.

- 594 Mu Cai, Jianwei Yang, Jianfeng Gao, and Yong Jae Lee. Matryoshka multimodal models. *arXiv*
595 *preprint arXiv:2405.17430*, 2024.
- 596
597 Junbum Cha, Wooyoung Kang, Jonghwan Mun, and Byungseok Roh. Honeybee: Locality-enhanced
598 projector for multimodal llm. In *CVPR*, 2024.
- 599 Jun Chen, Deyao Zhu, Xiaoqian Shen, Xiang Li, Zechun Liu, Pengchuan Zhang, Raghuraman
600 Krishnamoorthi, Vikas Chandra, Yunyang Xiong, and Mohamed Elhoseiny. Minigpt-v2: large
601 language model as a unified interface for vision-language multi-task learning. *arXiv preprint*
602 *arXiv:2310.09478*, 2023a.
- 603 Keqin Chen, Zhao Zhang, Weili Zeng, Richong Zhang, Feng Zhu, and Rui Zhao. Shikra: Unleashing
604 multimodal llm’s referential dialogue magic. *arXiv preprint arXiv:2306.15195*, 2023b.
- 605
606 Kezhen Chen, Rahul Thapa, Rahul Chalamala, Ben Athiwaratkun, Shuaiwen Leon Song, and James
607 Zou. Dragonfly: Multi-resolution zoom supercharges large visual-language model. *arXiv preprint*
608 *arXiv:2406.00977*, 2024a.
- 609 Lin Chen, Jisong Li, Xiaoyi Dong, Pan Zhang, Conghui He, Jiaqi Wang, Feng Zhao, and Dahua
610 Lin. Sharegpt4v: Improving large multi-modal models with better captions. *arXiv preprint*
611 *arXiv:2311.12793*, 2023c.
- 612
613 Wenhui Chen, Hongmin Wang, Jianshu Chen, Yunkai Zhang, Hong Wang, Shiyang Li, Xiyu Zhou,
614 and William Yang Wang. Tabfact: A large-scale dataset for table-based fact verification. *arXiv*
615 *preprint arXiv:1909.02164*, 2019.
- 616 Xinlei Chen, Hao Fang, Tsung-Yi Lin, Ramakrishna Vedantam, Saurabh Gupta, Piotr Dollár, and
617 C Lawrence Zitnick. Microsoft coco captions: Data collection and evaluation server. *arXiv preprint*
618 *arXiv:1504.00325*, 2015.
- 619 Zhe Chen, Weiyun Wang, Hao Tian, Shenglong Ye, Zhangwei Gao, Erfei Cui, Wenwen Tong, Kongzhi
620 Hu, Jiapeng Luo, Zheng Ma, et al. How far are we to gpt-4v? closing the gap to commercial
621 multimodal models with open-source suites. *arXiv preprint arXiv:2404.16821*, 2024b.
- 622
623 Zhe Chen, Jiannan Wu, Wenhui Wang, Weijie Su, Guo Chen, Sen Xing, Muyan Zhong, Qinglong
624 Zhang, Xizhou Zhu, Lewei Lu, et al. Internvl: Scaling up vision foundation models and aligning
625 for generic visual-linguistic tasks. In *CVPR*, 2024c.
- 626 Zhiyu Chen, Wenhui Chen, Charese Smiley, Sameena Shah, Iana Borova, Dylan Langdon, Reema
627 Moussa, Matt Beane, Ting-Hao Huang, Bryan Routledge, et al. Finqa: A dataset of numerical
628 reasoning over financial data. *arXiv preprint arXiv:2109.00122*, 2021.
- 629
630 Zesen Cheng, Sicong Leng, Hang Zhang, Yifei Xin, Xin Li, Guanzheng Chen, Yongxin Zhu, Wenqi
631 Zhang, Ziyang Luo, Deli Zhao, and Lidong Bing. VideoLLaMA 2: Advancing spatial-temporal
632 modeling and audio understanding in video-llms. *arXiv preprint arXiv:2406.07476*, 2024.
- 633 Zhoujun Cheng, Haoyu Dong, Zhiruo Wang, Ran Jia, Jiaqi Guo, Yan Gao, Shi Han, Jian-Guang
634 Lou, and Dongmei Zhang. Hitab: A hierarchical table dataset for question answering and natural
635 language generation. *arXiv preprint arXiv:2108.06712*, 2021.
- 636
637 Xiaoyi Dong, Pan Zhang, Yuhang Zang, Yuhang Cao, Bin Wang, Linke Ouyang, Songyang Zhang,
638 Haodong Duan, Wenwei Zhang, Yining Li, et al. Internlm-xcomposer2-4khd: A pioneering
639 large vision-language model handling resolutions from 336 pixels to 4k hd. *arXiv preprint*
640 *arXiv:2404.06512*, 2024a.
- 641
642 Xiaoyi Dong, Pan Zhang, Yuhang Zang, Yuhang Cao, Bin Wang, Linke Ouyang, Songyang Zhang,
643 Haodong Duan, Wenwei Zhang, Yining Li, et al. Internlm-xcomposer2-4khd: A pioneering
644 large vision-language model handling resolutions from 336 pixels to 4k hd. *arXiv preprint*
arXiv:2404.06512, 2024b.
- 645
646 Haodong Duan, Junming Yang, Yuxuan Qiao, Xinyu Fang, Lin Chen, Yuan Liu, Xiaoyi Dong, Yuhang
647 Zang, Pan Zhang, Jiaqi Wang, Dahua Lin, and Kai Chen. Vlmevalkit: An open-source toolkit
for evaluating large multi-modality models, 2024. URL <https://arxiv.org/abs/2407.11691>.

- 648 Abhimanyu Dubey, Abhinav Jauhri, Abhinav Pandey, Abhishek Kadian, Ahmad Al-Dahle, Aiesha
649 Letman, Akhil Mathur, Alan Schelten, Amy Yang, Angela Fan, et al. The llama 3 herd of models.
650 *arXiv preprint arXiv:2407.21783*, 2024.
- 651 Yunhao Fang, Ligeng Zhu, Yao Lu, Yan Wang, Pavlo Molchanov, Jang Hyun Cho, Marco Pavone,
652 Song Han, and Hongxu Yin. *vila²: Vila augmented vila*. *arXiv preprint arXiv:2407.17453*, 2024.
- 653 Maxwell Forbes, Christine Kaeser-Chen, Piyush Sharma, and Serge Belongie. Neural naturalist:
654 Generating fine-grained image comparisons. *arXiv preprint arXiv:1909.04101*, 2019.
- 655 Chaoyou Fu, Peixian Chen, Yunhang Shen, Yulei Qin, Mengdan Zhang, Xu Lin, Jinrui Yang, Xiawu
656 Zheng, Ke Li, Xing Sun, Yunsheng Wu, and Rongrong Ji. Mme: A comprehensive evaluation
657 benchmark for multimodal large language models. *arXiv preprint arXiv:2306.13394*, 2024a.
- 658 Chaoyou Fu, Yuhan Dai, Yondong Luo, Lei Li, Shuhuai Ren, Renrui Zhang, Zihan Wang, Chenyu
659 Zhou, Yunhang Shen, Mengdan Zhang, et al. Video-MME: The first-ever comprehensive evaluation
660 benchmark of multi-modal llms in video analysis. *arXiv preprint arXiv:2405.21075*, 2024b.
- 661 Stephanie Fu*, Netanel Tamir*, Shobhita Sundaram*, Lucy Chai, Richard Zhang, Tali Dekel, and
662 Phillip Isola. Dreamsim: Learning new dimensions of human visual similarity using synthetic data.
663 *arXiv preprint arXiv:2306.09344*, 2023.
- 664 Xingyu Fu, Yushi Hu, Bangzheng Li, Yu Feng, Haoyu Wang, Xudong Lin, Dan Roth, Noah A Smith,
665 Wei-Chiu Ma, and Ranjay Krishna. Blink: Multimodal large language models can see but not
666 perceive. *arXiv preprint arXiv:2404.12390*, 2024c.
- 667 Leo Gao, Jonathan Tow, Baber Abbasi, Stella Biderman, Sid Black, Anthony DiPofi, Charles Foster,
668 Laurence Golding, Jeffrey Hsu, Alain Le Noac’h, Haonan Li, Kyle McDonell, Niklas Muennighoff,
669 Chris Ociepa, Jason Phang, Laria Reynolds, Hailey Schoelkopf, Aviya Skowron, Lintang Sutawika,
670 Eric Tang, Anish Thite, Ben Wang, Kevin Wang, and Andy Zou. A framework for few-shot
671 language model evaluation, 12 2023. URL <https://zenodo.org/records/10256836>.
- 672 Peng Gao, Renrui Zhang, Chris Liu, Longtian Qiu, Siyuan Huang, Weifeng Lin, Shitian Zhao, Shijie
673 Geng, Ziyi Lin, Peng Jin, et al. Sphinx-x: Scaling data and parameters for a family of multi-modal
674 large language models. *arXiv preprint arXiv:2402.05935*, 2024.
- 675 Chunjiang Ge, Sijie Cheng, Ziming Wang, Jiale Yuan, Yuan Gao, Jun Song, Shiji Song, Gao Huang,
676 and Bo Zheng. Convllava: Hierarchical backbones as visual encoder for large multimodal models.
677 *arXiv preprint arXiv:2405.15738*, 2024.
- 678 Tom Gunter, Zirui Wang, Chong Wang, Ruoming Pang, Andy Narayanan, Aonan Zhang, Bowen
679 Zhang, Chen Chen, Chung-Cheng Chiu, David Qiu, et al. Apple intelligence foundation language
680 models. *arXiv preprint arXiv:2407.21075*, 2024.
- 681 Agrim Gupta, Piotr Dollár, and Ross B. Girshick. LVIS: A dataset for large vocabulary instance
682 segmentation. In *CVPR*, 2019.
- 683 MUYANG HE, YEXIN LIU, BOYA WU, JIANHAO YUAN, YUEZE WANG, TIEJUN HUANG, and BO ZHAO. Efficient
684 multimodal learning from data-centric perspective. *arXiv preprint arXiv:2402.11530*, 2024.
- 685 Musashi Hinck, Matthew L Olson, David Cobbley, Shao-Yen Tseng, and Vasudev Lal. Llava-gemma:
686 Accelerating multimodal foundation models with a compact language model. *arXiv preprint*
687 *arXiv:2404.01331*, 2024.
- 688 Wenyi Hong, Weihang Wang, Ming Ding, Wenmeng Yu, Qingsong Lv, Yan Wang, Yean Cheng,
689 Shiyu Huang, Junhui Ji, Zhao Xue, et al. Cogvlm2: Visual language models for image and video
690 understanding. *arXiv preprint arXiv:2408.16500*, 2024a.
- 691 Wenyi Hong, Weihang Wang, Qingsong Lv, Jiazhen Xu, Wenmeng Yu, Junhui Ji, Yan Wang, Zihan
692 Wang, Yuxiao Dong, Ming Ding, et al. Cogagent: A visual language model for gui agents. In
693 *CVPR*, 2024b.
- 694 Yu-Chung Hsiao, Fedir Zubach, Maria Wang, and Jindong Chen. Screenqa: Large-scale question-
695 answer pairs over mobile app screenshots. *arXiv preprint arXiv:2209.08199*, 2022.

- 702 Anwen Hu, Haiyang Xu, Jiabo Ye, Ming Yan, Liang Zhang, Bo Zhang, Chen Li, Ji Zhang, Qin Jin, Fei
703 Huang, et al. mplug-docowl 1.5: Unified structure learning for ocr-free document understanding.
704 *arXiv preprint arXiv:2403.12895*, 2024a.
- 705 Anwen Hu, Haiyang Xu, Jiabo Ye, Ming Yan, Liang Zhang, Bo Zhang, Chen Li, Ji Zhang, Qin Jin, Fei
706 Huang, et al. mplug-docowl 1.5: Unified structure learning for ocr-free document understanding.
707 *arXiv preprint arXiv:2403.12895*, 2024b.
- 708
- 709 Mingxin Huang, Yuliang Liu, Ding kang Liang, Lianwen Jin, and Xiang Bai. Mini-monkey: Alleviate
710 the sawtooth effect by multi-scale adaptive cropping. *arXiv preprint arXiv:2408.02034*, 2024.
- 711 Shaohan Huang, Li Dong, Wenhui Wang, Yaru Hao, Saksham Singhal, Shuming Ma, Tengchao Lv,
712 Lei Cui, Owais Khan Mohammed, Barun Patra, et al. Language is not all you need: Aligning
713 perception with language models. *NeurIPS*, 2023.
- 714
- 715 Drew A Hudson and Christopher D Manning. Gqa: A new dataset for real-world visual reasoning
716 and compositional question answering. *CVPR*, 2019.
- 717 Raisa Islam and Owana Marzia Moushi. Gpt-4o: The cutting-edge advancement in multimodal llm.
718 *Authorea Preprints*, 2024.
- 719
- 720 Harsh Jhamtani and Taylor Berg-Kirkpatrick. Learning to describe differences between pairs of
721 similar images. *arXiv preprint arXiv:1808.10584*, 2018.
- 722 Dongfu Jiang, Xuan He, Huaye Zeng, Cong Wei, Max Ku, Qian Liu, and Wenhui Chen. Mantis:
723 Interleaved multi-image instruction tuning. *arXiv preprint arXiv:2405.01483*, 2024.
- 724
- 725 Peng Jin, Ryuichi Takano, Wancai Zhang, Xiaochun Cao, and Li Yuan. Chat-univi: Unified visual
726 representation empowers large language models with image and video understanding. In *CVPR*,
727 2024a.
- 728 Yizhang Jin, Jian Li, Yexin Liu, Tianjun Gu, Kai Wu, Zhengkai Jiang, Muyang He, Bo Zhao, Xin
729 Tan, Zhenye Gan, et al. Efficient multimodal large language models: A survey. *arXiv preprint*
730 *arXiv:2405.10739*, 2024b.
- 731 Justin Johnson, Bharath Hariharan, Laurens Van Der Maaten, Li Fei-Fei, C Lawrence Zitnick, and
732 Ross Girshick. Clevr: A diagnostic dataset for compositional language and elementary visual
733 reasoning. In *CVPR*, 2017.
- 734
- 735 Kushal Kafle, Brian Price, Scott Cohen, and Christopher Kanan. Dvqa: Understanding data visualiza-
736 tions via question answering. In *CVPR*, 2018.
- 737 Mehran Kazemi, Hamidreza Alvani, Ankit Anand, Jialin Wu, Xi Chen, and Radu Soricut. Geomverse:
738 A systematic evaluation of large models for geometric reasoning. *arXiv preprint arXiv:2312.12241*,
739 2023.
- 740 Sahar Kazemzadeh, Vicente Ordonez, Mark Matten, and Tamara Berg. Referitgame: Referring to
741 objects in photographs of natural scenes. In *EMNLP*, 2014.
- 742
- 743 Aniruddha Kembhavi, Mike Salvato, Eric Kolve, Minjoon Seo, Hannaneh Hajishirzi, and Ali Farhadi.
744 A diagram is worth a dozen images. In *ECCV*, 2016a.
- 745 Aniruddha Kembhavi, Mike Salvato, Eric Kolve, Minjoon Seo, Hannaneh Hajishirzi, and Ali Farhadi.
746 A diagram is worth a dozen images. In *ECCV*, 2016b.
- 747
- 748 Geewook Kim, Teakgyu Hong, Moonbin Yim, JeongYeon Nam, Jinyoung Park, Jinyeong Yim,
749 Wonseok Hwang, Sangdoon Yun, Dongyoon Han, and Seunghyun Park. Ocr-free document
750 understanding transformer. In *ECCV*, 2022.
- 751 Wonkyun Kim, Changin Choi, Wonseok Lee, and Wonjong Rhee. An image grid can be worth a
752 video: Zero-shot video question answering using a vlm. *arXiv preprint arXiv:2403.18406*, 2024.
- 753
- 754 Ranjay Krishna, Yuke Zhu, Oliver Groth, Justin Johnson, Kenji Hata, Joshua Kravitz, Stephanie
755 Chen, Yannis Kalantidis, Li-Jia Li, David A Shamma, et al. Visual genome: Connecting language
and vision using crowdsourced dense image annotations. *IJCV*, 2017.

- 756 Xin Lai, Zhuotao Tian, Yukang Chen, Yanwei Li, Yuhui Yuan, Shu Liu, and Jiaya Jia. Lisa: Reasoning
757 segmentation via large language model. In *CVPR*, 2024.
- 758
- 759 Hugo Laurençon, Andrés Marafioti, Victor Sanh, and Léo Tronchon. Building and better under-
760 standing vision-language models: insights and future directions. *arXiv preprint arXiv:2408.12637*,
761 2024a.
- 762 Hugo Laurençon, Lucile Saulnier, Léo Tronchon, Stas Bekman, Amanpreet Singh, Anton Lozhkov,
763 Thomas Wang, Siddharth Karamcheti, Alexander Rush, Douwe Kiela, et al. Obelics: An open
764 web-scale filtered dataset of interleaved image-text documents. *NeurIPS*, 2024b.
- 765
- 766 Hugo Laurençon, Léo Tronchon, Matthieu Cord, and Victor Sanh. What matters when building
767 vision-language models? *arXiv preprint arXiv:2405.02246*, 2024a.
- 768
- 769 Hugo Laurençon, Léo Tronchon, and Victor Sanh. Unlocking the conversion of web screenshots into
770 html code with the websight dataset. *arXiv preprint arXiv:2403.09029*, 2024b.
- 771 Dmitry Lepikhin, HyoukJoong Lee, Yuanzhong Xu, Dehao Chen, Orhan Firat, Yanping Huang,
772 Maxim Krikun, Noam Shazeer, and Zhifeng Chen. {GS}hard: Scaling giant models with condi-
773 tional computation and automatic sharding. In *ICLR*, 2021.
- 774
- 775 Bo Li, Yuanhan Zhang, Liangyu Chen, Jinghao Wang, Fanyi Pu, Jingkang Yang, Chunyuan Li, and
776 Ziwei Liu. Mimic-it: Multi-modal in-context instruction tuning. *arXiv preprint arXiv:2306.05425*,
777 2023a.
- 778 Bo Li, Hao Zhang, Kaichen Zhang, Dong Guo, Yuanhan Zhang, Renrui Zhang, Feng
779 Li, Ziwei Liu, and Chunyuan Li. Llava-next: What else influences visual instruc-
780 tion tuning beyond data?, May 2024a. URL [https://llava-vl.github.io/blog/
781 2024-05-25-llava-next-ablations/](https://llava-vl.github.io/blog/2024-05-25-llava-next-ablations/).
- 782
- 783 Bo Li, Peiyuan Zhang, Kaichen Zhang, Fanyi Pu, Xinrun Du, Yuhao Dong, Haotian Liu, Yuanhan
784 Zhang, Ge Zhang, Chunyuan Li, and Ziwei Liu. Lmms-eval: Accelerating the development of large
785 multimodal models, March 2024b. URL [https://github.com/EvolvingLMMS-Lab/
786 lmms-eval](https://github.com/EvolvingLMMS-Lab/lmms-eval).
- 787 Bo Li, Yuanhan Zhang, Dong Guo, Renrui Zhang, Feng Li, Hao Zhang, Kaichen Zhang, Yanwei
788 Li, Ziwei Liu, and Chunyuan Li. Llava-onevision: Easy visual task transfer. *arXiv preprint
789 arXiv:2408.03326*, 2024c.
- 790 Bohao Li, Rui Wang, Guangzhi Wang, Yuying Ge, Yixiao Ge, and Ying Shan. Seed-bench: Bench-
791 marking multimodal llms with generative comprehension. *arXiv preprint arXiv:2307.16125*,
792 2023b.
- 793
- 794 Chunyuan Li, Zhe Gan, Zhengyuan Yang, Jianwei Yang, Linjie Li, Lijuan Wang, Jianfeng Gao, et al.
795 Multimodal foundation models: From specialists to general-purpose assistants. *Foundations and
796 Trends® in Computer Graphics and Vision*, 16(1-2):1–214, 2024d.
- 797
- 798 Feng Li, Renrui Zhang, Hao Zhang, Yuanhan Zhang, Bo Li, Wei Li, Zejun Ma, and Chunyuan Li.
799 Llava-next-interleave: Tackling multi-image, video, and 3d in large multimodal models. *arXiv
800 preprint arXiv:2407.07895*, 2024e.
- 801
- 802 Feng Li, Renrui Zhang, Hao Zhang, Yuanhan Zhang, Bo Li, Wei Li, Zejun Ma,
803 and Chunyuan Li. Llava-next: Tackling multi-image, video, and 3d in large
804 multimodal models, June 2024f. URL [https://llava-vl.github.io/blog/
2024-06-16-llava-next-interleave/](https://llava-vl.github.io/blog/2024-06-16-llava-next-interleave/).
- 805
- 806 Gang Li and Yang Li. Spotlight: Mobile UI understanding using vision-language models with a
807 focus. In *ICLR*, 2023.
- 808
- 809 Jiachen Li, Xinyao Wang, Sijie Zhu, Chia-Wen Kuo, Lu Xu, Fan Chen, Jitesh Jain, Humphrey Shi,
and Longyin Wen. Cumo: Scaling multimodal llm with co-upcycled mixture-of-experts. *arXiv
preprint arXiv:2405.05949*, 2024g.

- 810 Jiapeng Li, Ping Wei, Wenjuan Han, and Lifeng Fan. IntentQA: Context-aware video intent reasoning.
811 In *ICCV*, 2023c.
- 812
- 813 Junnan Li, Dongxu Li, Silvio Savarese, and Steven Hoi. Blip-2: Bootstrapping language-image
814 pre-training with frozen image encoders and large language models. In *ICML*, 2023d.
- 815
- 816 KunChang Li, Yinan He, Yi Wang, Yizhuo Li, Wenhai Wang, Ping Luo, Yali Wang, Limin Wang, and
817 Yu Qiao. Videochat: Chat-centric video understanding. *arXiv preprint arXiv:2305.06355*, 2023e.
- 818
- 819 Kunchang Li, Yali Wang, Yinan He, Yizhuo Li, Yi Wang, Yi Liu, Zun Wang, Jilan Xu, Guo Chen, Ping
820 Luo, Limin Wang, and Yu Qiao. Mvbench: A comprehensive multi-modal video understanding
821 benchmark. *arXiv preprint arXiv:2311.17005*, 2023f.
- 822
- 823 Kunchang Li, Yali Wang, Yinan He, Yizhuo Li, Yi Wang, Yi Liu, Zun Wang, Jilan Xu, Guo Chen,
824 Ping Luo, et al. Mvbench: A comprehensive multi-modal video understanding benchmark. In
CVPR, 2024h.
- 825
- 826 Lei Li, Yuqi Wang, Runxin Xu, Peiyi Wang, Xiachong Feng, Lingpeng Kong, and Qi Liu. Multimodal
827 arxiv: A dataset for improving scientific comprehension of large vision-language models. *arXiv
828 preprint arXiv:2403.00231*, 2024i.
- 829
- 830 Qingyun Li, Zhe Chen, Weiyun Wang, Wenhai Wang, Shenglong Ye, Zhenjiang Jin, Guanzhou Chen,
831 Yinan He, Zhangwei Gao, Erfei Cui, et al. Omnicorpus: An unified multimodal corpus of 10
billion-level images interleaved with text. *arXiv preprint arXiv:2406.08418*, 2024j.
- 832
- 833 Wentong Li, Yuqian Yuan, Jian Liu, Dongqi Tang, Song Wang, Jianke Zhu, and Lei Zhang. Token-
834 packer: Efficient visual projector for multimodal llm. *arXiv preprint arXiv:2407.02392*, 2024k.
- 835
- 836 Yang Li, Gang Li, Luheng He, Jingjie Zheng, Hong Li, and Zhiwei Guan. Widget captioning:
837 Generating natural language description for mobile user interface elements. In Bonnie Webber,
Trevor Cohn, Yulan He, and Yang Liu (eds.), *EMNLP*, 2020.
- 838
- 839 Yanwei Li, Chengyao Wang, and Jiaya Jia. LLaMA-VID: An image is worth 2 tokens in large
840 language models. *arXiv preprint arXiv:2311.17043*, 2023g.
- 841
- 842 Yanwei Li, Yuechen Zhang, Chengyao Wang, Zhisheng Zhong, Yixin Chen, Ruihang Chu, Shaoteng
843 Liu, and Jiaya Jia. Mini-gemini: Mining the potential of multi-modality vision language models.
arXiv preprint arXiv:2403.18814, 2024l.
- 844
- 845 Yifan Li, Yifan Du, Kun Zhou, Jinpeng Wang, Wayne Xin Zhao, and Ji-Rong Wen. Evaluating object
846 hallucination in large vision-language models. *arXiv preprint arXiv:2305.10355*, 2023h.
- 847
- 848 Zhang Li, Biao Yang, Qiang Liu, Zhiyin Ma, Shuo Zhang, Jingxu Yang, Yabo Sun, Yuliang Liu, and
849 Xiang Bai. Monkey: Image resolution and text label are important things for large multi-modal
models. *arXiv preprint arXiv:2311.06607*, 2023i.
- 850
- 851 Wing Lian, Bleys Goodson, Eugene Pentland, Austin Cook, Chanvichet Vong, and "Teknum".
852 Openorca: An open dataset of gpt augmented flan reasoning traces. <https://huggingface.co/Open-Orca/OpenOrca>, 2023.
- 853
- 854 Bin Lin, Bin Zhu, Yang Ye, Munan Ning, Peng Jin, and Li Yuan. Video-llava: Learning united visual
855 representation by alignment before projection. *arXiv preprint arXiv:2311.10122*, 2023a.
- 856
- 857 Bin Lin, Zhenyu Tang, Yang Ye, Jiayi Cui, Bin Zhu, Peng Jin, Junwu Zhang, Munan Ning, and
858 Li Yuan. Moe-llava: Mixture of experts for large vision-language models. *arXiv preprint
859 arXiv:2401.15947*, 2024a.
- 860
- 861 Ji Lin, Hongxu Yin, Wei Ping, Pavlo Molchanov, Mohammad Shoeybi, and Song Han. Vila: On
862 pre-training for visual language models. In *CVPR*, 2024b.
- 863
- Tsung-Yi Lin, Michael Maire, Serge Belongie, James Hays, Pietro Perona, Deva Ramanan, Piotr
Dollár, and C Lawrence Zitnick. Microsoft coco: Common objects in context. In *ECCV*, 2014.

- 864 Ziyi Lin, Chris Liu, Renrui Zhang, Peng Gao, Longtian Qiu, Han Xiao, Han Qiu, Chen Lin, Wenqi
865 Shao, Keqin Chen, et al. Sphinx: The joint mixing of weights, tasks, and visual embeddings for
866 multi-modal large language models. *arXiv preprint arXiv:2311.07575*, 2023b.
- 867
868 Haotian Liu, Chunyuan Li, Yuheng Li, and Yong Jae Lee. Llava-1.5: Improved baselines with visual
869 instruction tuning. *arXiv preprint arXiv:2310.03744*, 2023a.
- 870
871 Haotian Liu, Chunyuan Li, Qingyang Wu, and Yong Jae Lee. Visual instruction tuning. *arXiv
872 preprint arXiv:2304.08485*, 2023b.
- 873
874 Haotian Liu, Chunyuan Li, Yuheng Li, Bo Li, Yuanhan Zhang, Sheng Shen, and Yong Jae Lee.
875 Llava-next: Improved reasoning, ocr, and world knowledge, 2024a.
- 876
877 Yuliang Liu, Zhang Li, Mingxin Huang, Biao Yang, Wenwen Yu, Chunyuan Li, Xucheng Yin, Cheng
878 lin Liu, Lianwen Jin, and Xiang Bai. On the hidden mystery of ocr in large multimodal models.
879 *arXiv preprint arXiv:2305.07895*, 2024b.
- 880
881 Haoyu Lu, Wen Liu, Bo Zhang, Bingxuan Wang, Kai Dong, Bo Liu, Jingxiang Sun, Tongzheng Ren,
882 Zhuoshu Li, Hao Yang, Yaofeng Sun, Chengqi Deng, Hanwei Xu, Zhenda Xie, and Chong Ruan.
883 Deepseek-vl: Towards real-world vision-language understanding. *arXiv preprint arXiv:2403.05525*,
884 2024.
- 885
886 Pan Lu, Ran Gong, Shibiao Jiang, Liang Qiu, Siyuan Huang, Xiaodan Liang, and Song-Chun Zhu.
887 Inter-gps: Interpretable geometry problem solving with formal language and symbolic reasoning.
888 In *ACL*, 2021a.
- 889
890 Pan Lu, Liang Qiu, Jiaqi Chen, Tony Xia, Yizhou Zhao, Wei Zhang, Zhou Yu, Xiaodan Liang,
891 and Song-Chun Zhu. Iconqa: A new benchmark for abstract diagram understanding and visual
892 language reasoning. In *NeurIPS Track on Datasets and Benchmarks*, 2021b.
- 893
894 Pan Lu, Swaroop Mishra, Tony Xia, Liang Qiu, Kai-Wei Chang, Song-Chun Zhu, Oyvind Taffjord,
895 Peter Clark, and Ashwin Kalyan. Learn to explain: Multimodal reasoning via thought chains for
896 science question answering. In *NeurIPS*, 2022.
- 897
898 Pan Lu, Hritik Bansal, Tony Xia, Jiacheng Liu, Chunyuan Li, Hannaneh Hajishirzi, Hao Cheng,
899 Kai-Wei Chang, Michel Galley, and Jianfeng Gao. Mathvista: Evaluating mathematical reasoning
900 of foundation models in visual contexts. *arXiv preprint arXiv:2310.02255*, 2023a.
- 901
902 Pan Lu, Liang Qiu, Kai-Wei Chang, Ying Nian Wu, Song-Chun Zhu, Tanmay Rajpurohit, Peter
903 Clark, and Ashwin Kalyan. Dynamic prompt learning via policy gradient for semi-structured
904 mathematical reasoning. In *ICLR*, 2023b.
- 905
906 Ziyang Luo, Can Xu, Pu Zhao, Qingfeng Sun, Xiubo Geng, Wenxiang Hu, Chongyang Tao, Jing
907 Ma, Qingwei Lin, and Daxin Jiang. Wizardcoder: Empowering code large language models with
908 evol-instruct. *arXiv preprint arXiv:2306.08568*, 2023.
- 909
910 Fan Ma, Xiaojie Jin, Heng Wang, Yuchen Xian, Jiashi Feng, and Yi Yang. Vista-llama: Reducing
911 hallucination in video language models via equal distance to visual tokens. In *CVPR*, 2024.
- 912
913 Muhammad Maaz, Hanoona Rasheed, Salman Khan, and Fahad Shahbaz Khan. Video-ChatGPT:
914 Towards detailed video understanding via large vision and language models. In *ACL*, 2024.
- 915
916 Kartikeya Mangalam, Raiymbek Akshulakov, and Jitendra Malik. Egoschema: A diagnostic
917 benchmark for very long-form video language understanding. *NeurIPS*, 2024.
- 918
919 Kenneth Marino, Mohammad Rastegari, Ali Farhadi, and Roozbeh Mottaghi. Ok-vqa: A visual
920 question answering benchmark requiring external knowledge. In *CVPR*, 2019.
- 921
922 Ahmed Masry, Do Xuan Long, Jia Qing Tan, Shafiq Joty, and Enamul Hoque. Chartqa: A bench-
923 mark for question answering about charts with visual and logical reasoning. *arXiv preprint
924 arXiv:2203.10244*, 2022.
- 925
926 Minesh Mathew, Dimosthenis Karatzas, and CV Jawahar. Docvqa: A dataset for vqa on document
927 images. In *WACV*, 2021.

- 918 Minesh Mathew, Viraj Bagal, Rubèn Tito, Dimosthenis Karatzas, Ernest Valveny, and CV Jawahar.
919 Infographicvqa. In *WACV*, 2022.
920
- 921 Brandon McKinzie, Zhe Gan, Jean-Philippe Fauconnier, Sam Dodge, Bowen Zhang, Philipp Dufter,
922 Dhruvi Shah, Xianzhi Du, Futang Peng, Floris Weers, et al. Mm1: Methods, analysis & insights
923 from multimodal llm pre-training. *arXiv preprint arXiv:2403.09611*, 2024.
- 924 Lingchen Meng, Jianwei Yang, Rui Tian, Xiyang Dai, Zuxuan Wu, Jianfeng Gao, and Yu-Gang Jiang.
925 Deepstack: Deeply stacking visual tokens is surprisingly simple and effective for lms. *arXiv*
926 *preprint arXiv:2406.04334*, 2024.
927
- 928 C Mike, H Matt, M Ankit, X Jianwei, W Jun, S Sam, G Ali, W Patrick, Z Matei, and X Reynold.
929 Free dolly: Introducing the world’s first truly open instruction-tuned llm, 2023.
- 930 Anand Mishra, Shashank Shekhar, Ajeet Kumar Singh, and Anirban Chakraborty. Ocr-vqa: Visual
931 question answering by reading text in images. In *ICDAR*, 2019.
932
- 933 Arindam Mitra, Hamed Khanpour, Corby Rosset, and Ahmed Awadallah. Orca-math: Unlocking the
934 potential of slms in grade school math. *arXiv preprint arXiv:2402.14830*, 2024.
935
- 936 Varun K Nagaraja, Vlad I Morariu, and Larry S Davis. Modeling context between objects for referring
937 expression understanding. In *ECCV*, 2016.
- 938 Jason Obeid and Enamul Hoque. Chart-to-text: Generating natural language descriptions for charts
939 by adapting the transformer model. *arXiv preprint arXiv:2010.09142*, 2020.
940
- 941 OpenAI. Gpt-4 vision. OpenAI, 2024. [https://openai.com/research/
942 gpt-4-vision](https://openai.com/research/gpt-4-vision).
- 943 Panupong Pasupat and Percy Liang. Compositional semantic parsing on semi-structured tables. *arXiv*
944 *preprint arXiv:1508.00305*, 2015.
945
- 946 Zhiliang Peng, Wenhui Wang, Li Dong, Yaru Hao, Shaohan Huang, Shuming Ma, and Furu
947 Wei. Kosmos-2: Grounding multimodal large language models to the world. *arXiv preprint*
948 *arXiv:2306.14824*, 2023.
949
- 950 Bryan A Plummer, Liwei Wang, Chris M Cervantes, Juan C Caicedo, Julia Hockenmaier, and
951 Svetlana Lazebnik. Flickr30k entities: Collecting region-to-phrase correspondences for richer
952 image-to-sentence models. In *ICCV*, 2015.
- 953 Hanoona Rasheed, Muhammad Maaz, Sahal Shaji, Abdelrahman Shaker, Salman Khan, Hisham
954 Cholakkal, Rao M Anwer, Eric Xing, Ming-Hsuan Yang, and Fahad S Khan. Glamm: Pixel
955 grounding large multimodal model. In *CVPR*, 2024.
956
- 957 Machel Reid, Nikolay Savinov, Denis Teplyashin, Dmitry Lepikhin, Timothy Lillicrap, Jean-baptiste
958 Alayrac, Radu Soricut, Angeliki Lazaridou, Orhan Firat, Julian Schrittwieser, et al. Gemini
959 1.5: Unlocking multimodal understanding across millions of tokens of context. *arXiv preprint*
960 *arXiv:2403.05530*, 2024.
- 961 Zhongwei Ren, Zhicheng Huang, Yunchao Wei, Yao Zhao, Dongmei Fu, Jiashi Feng, and Xiaojie Jin.
962 Pixellm: Pixel reasoning with large multimodal model. In *CVPR*, 2024.
963
- 964 Eldon Schoop, Xin Zhou, Gang Li, Zhouong Chen, Bjoern Hartmann, and Yang Li. Predicting and
965 explaining mobile ui tappability with vision modeling and saliency analysis. In *Proceedings of*
966 *the 2022 CHI Conference on Human Factors in Computing Systems*. Association for Computing
967 Machinery, 2022.
- 968 Dustin Schwenk, Apoorv Khandelwal, Christopher Clark, Kenneth Marino, and Roozbeh Mottaghi.
969 A-okvqa: A benchmark for visual question answering using world knowledge. In *ECCV*, 2022.
970
- 971 Shuai Shao, Zeming Li, Tianyuan Zhang, Chao Peng, Gang Yu, Xiangyu Zhang, Jing Li, and Jian
Sun. Objects365: A large-scale, high-quality dataset for object detection. In *ICCV*, 2019.

- 972 Min Shi, Fuxiao Liu, Shihao Wang, Shijia Liao, Subhashree Radhakrishnan, De-An Huang, Hongxu
973 Yin, Karan Sapra, Yaser Yacoob, Humphrey Shi, et al. Eagle: Exploring the design space for
974 multimodal llms with mixture of encoders. *arXiv preprint arXiv:2408.15998*, 2024.
- 975 Chenglei Si, Yanzhe Zhang, Zhengyuan Yang, Ruibo Liu, and Diyi Yang. Design2code: How far are
976 we from automating front-end engineering? *arXiv preprint arXiv:2403.03163*, 2024.
- 977
- 978 Oleksii Sidorov, Ronghang Hu, Marcus Rohrbach, and Amanpreet Singh. Textcaps: a dataset for
979 image captioning with reading comprehension. In *ECCV*, 2020.
- 980
- 981 Amanpreet Singh, Vivek Natarajan, Meet Shah, Yu Jiang, Xinlei Chen, Dhruv Batra, Devi Parikh,
982 and Marcus Rohrbach. Towards vqa models that can read. In *CVPR*, 2019.
- 983
- 984 Enxin Song, Wenhao Chai, Tian Ye, Jenq-Neng Hwang, Xi Li, and Gaoang Wang. Moviechat+:
985 Question-aware sparse memory for long video question answering. *arXiv preprint*
986 *arXiv:2404.17176*, 2024.
- 987
- 988 Tomasz Stanisławek, Filip Graliński, Anna Wróblewska, Dawid Lipiński, Agnieszka Kaliska, Paulina
989 Rosalska, Bartosz Topolski, and Przemysław Biecek. Kleister: key information extraction datasets
990 involving long documents with complex layouts. In *International Conference on Document*
991 *Analysis and Recognition*, 2021.
- 992
- 993 Alane Suhr, Stephanie Zhou, Ally Zhang, Iris Zhang, Huajun Bai, and Yoav Artzi. A corpus for
994 reasoning about natural language grounded in photographs. *arXiv preprint arXiv:1811.00491*,
995 2018.
- 996
- 997 Quan Sun, Yufeng Cui, Xiaosong Zhang, Fan Zhang, Qiyong Yu, Zhengxiong Luo, Yueze Wang,
998 Yongming Rao, Jingjing Liu, Tiejun Huang, and Xinlong Wang. Generative multimodal models
999 are in-context learners. *arXiv preprint arXiv:2312.13286*, 2023a.
- 1000
- 1001 Quan Sun, Qiyong Yu, Yufeng Cui, Fan Zhang, Xiaosong Zhang, Yueze Wang, Hongcheng Gao,
1002 Jingjing Liu, Tiejun Huang, and Xinlong Wang. Generative pretraining in multimodality. *arXiv*
1003 *preprint arXiv:2307.05222*, 2023b.
- 1004
- 1005 Quan Sun, Yufeng Cui, Xiaosong Zhang, Fan Zhang, Qiyong Yu, Yueze Wang, Yongming Rao,
1006 Jingjing Liu, Tiejun Huang, and Xinlong Wang. Generative multimodal models are in-context
1007 learners. In *CVPR*, 2024.
- 1008
- 1009 Stacey Svetlichnaya. Deepform: Understand structured documents at scale, 2020.
- 1010
- 1011 Ryota Tanaka, Kyosuke Nishida, and Sen Yoshida. Visualmrc: Machine reading comprehension on
1012 document images. In *AAAI*, 2021.
- 1013
- 1014 Benny J. Tang, Angie Boggust, and Arvind Satyanarayan. VisText: A Benchmark for Semantically
1015 Rich Chart Captioning. In *ACL*, 2023.
- 1016
- 1017 Jingqun Tang, Chunhui Lin, Zhen Zhao, Shu Wei, Binghong Wu, Qi Liu, Hao Feng, Yang Li, Siqi
1018 Wang, Lei Liao, et al. Textsquare: Scaling up text-centric visual instruction tuning. *arXiv preprint*
1019 *arXiv:2404.12803*, 2024.
- 1020
- 1021 Gemini Team, Rohan Anil, Sebastian Borgeaud, Yonghui Wu, Jean-Baptiste Alayrac, Jiahui Yu, Radu
1022 Soricut, Johan Schalkwyk, Andrew M Dai, Anja Hauth, et al. Gemini: a family of highly capable
1023 multimodal models. *arXiv preprint arXiv:2312.11805*, 2023.
- 1024
- 1025 Qwen team. Qwen2-vl, August 2024. URL <https://qwenlm.github.io/blog/qwen2-vl/>.
- 1026
- 1027 Shengbang Tong, Ellis Brown, Penghao Wu, Sanghyun Woo, Manoj Middepogu, Sai Charitha Akula,
1028 Jihan Yang, Shusheng Yang, Adithya Iyer, Xichen Pan, Austin Wang, Rob Fergus, Yann LeCun,
1029 and Saining Xie. Cambrian-1: A fully open, vision-centric exploration of multimodal llms. *arXiv*
1030 *preprint arXiv:2406.16860*, 2024a.
- 1031
- 1032 Shengbang Tong, Zhuang Liu, Yuexiang Zhai, Yi Ma, Yann LeCun, and Saining Xie. Eyes wide
1033 shut? exploring the visual shortcomings of multimodal llms. In *CVPR*, 2024b.

- 1026 Maria Tsimpoukelli, Jacob L Menick, Serkan Cabi, SM Eslami, Oriol Vinyals, and Felix Hill.
1027 Multimodal few-shot learning with frozen language models. *NeurIPS*, 2021.
1028
- 1029 Bryan Wang, Gang Li, Xin Zhou, Zhourong Chen, Tovi Grossman, and Yang Li. Screen2words: Au-
1030 tomatic mobile ui summarization with multimodal learning. In *The 34th Annual ACM Symposium*
1031 *on User Interface Software and Technology*. Association for Computing Machinery, 2021.
- 1032 Fei Wang, Xingyu Fu, James Y Huang, Zekun Li, Qin Liu, Xiaogeng Liu, Mingyu Derek Ma, Nan Xu,
1033 Wenxuan Zhou, Kai Zhang, et al. Muirbench: A comprehensive benchmark for robust multi-image
1034 understanding. *arXiv preprint arXiv:2406.09411*, 2024.
- 1035 Weihan Wang, Qingsong Lv, Wenmeng Yu, Wenyi Hong, Ji Qi, Yan Wang, Junhui Ji, Zhuoyi Yang,
1036 Lei Zhao, Xixuan Song, et al. Cogvlm: Visual expert for pretrained language models. *arXiv*
1037 *preprint arXiv:2311.03079*, 2023a.
- 1038
- 1039 Wenhai Wang, Zhe Chen, Xiaokang Chen, Jiannan Wu, Xizhou Zhu, Gang Zeng, Ping Luo, Tong
1040 Lu, Jie Zhou, Yu Qiao, et al. Visionllm: Large language model is also an open-ended decoder for
1041 vision-centric tasks. *arXiv preprint arXiv:2305.11175*, 2023b.
- 1042
- 1043 Bo Wu, Shoubin Yu, Zhenfang Chen, Joshua B Tenenbaum, and Chuang Gan. Star: A benchmark for
1044 situated reasoning in real-world videos. *arXiv preprint arXiv:2405.09711*, 2024a.
- 1045
- 1046 Haoning Wu, Hanwei Zhu, Zicheng Zhang, Erli Zhang, Chaofeng Chen, Liang Liao, Chunyi Li,
1047 Annan Wang, Wenxiu Sun, Qiong Yan, et al. Towards open-ended visual quality comparison.
1048 *arXiv preprint arXiv:2402.16641*, 2024b.
- 1049
- 1050 x.ai. Grok-1.5 vision preview. URL <https://x.ai/blog/grok-1.5v>.
- 1051
- 1052 Junbin Xiao, Xindi Shang, Angela Yao, and Tat-Seng Chua. NExT-QA: Next phase of question-
1053 answering to explaining temporal actions. In *CVPR*, 2021a.
- 1054
- 1055 Junbin Xiao, Xindi Shang, Angela Yao, and Tat-Seng Chua. Next-qa: Next phase of question-
1056 answering to explaining temporal actions. In *CVPR*, 2021b.
- 1057
- 1058 Lin Xu, Yilin Zhao, Daquan Zhou, Zhijie Lin, See Kiong Ng, and Jiashi Feng. Pllava: Parameter-free
1059 llava extension from images to videos for video dense captioning. *arXiv preprint arXiv:2404.16994*,
1060 2024a.
- 1061
- 1062 Mingze Xu, Mingfei Gao, Zhe Gan, Hong-You Chen, Zhengfeng Lai, Haiming Gang, Kai Kang,
1063 and Afshin Dehghan. SlowFast-LLaVA: A strong training-free baseline for video large language
1064 models. *arXiv preprint arXiv:2407.15841*, 2024b.
- 1065
- 1066 Ruyi Xu, Yuan Yao, Zonghao Guo, Junbo Cui, Zanlin Ni, Chunjiang Ge, Tat-Seng Chua, Zhiyuan Liu,
1067 Maosong Sun, and Gao Huang. Llava-uhd: an lmm perceiving any aspect ratio and high-resolution
1068 images. *arXiv preprint arXiv:2403.11703*, 2024c.
- 1069
- 1070 Le Xue, Manli Shu, Anas Awadalla, Jun Wang, An Yan, Senthil Purushwalkam, Honglu Zhou, Viraj
1071 Prabhu, Yutong Dai, Michael S Ryoo, et al. xgen-mm (blip-3): A family of open large multimodal
1072 models. *arXiv preprint arXiv:2408.08872*, 2024.
- 1073
- 1074 Jianwei Yang, Hao Zhang, Feng Li, Xueyan Zou, Chunyuan Li, and Jianfeng Gao. Set-of-mark
1075 prompting unleashes extraordinary visual grounding in gpt-4v. *arXiv preprint arXiv:2310.11441*,
1076 2023.
- 1077
- 1078 Huanjin Yao, Wenhao Wu, Taojiannan Yang, YuXin Song, Mengxi Zhang, Haocheng Feng, Yifan
1079 Sun, Zhiheng Li, Wanli Ouyang, and Jingdong Wang. Dense connector for mllms. *arXiv preprint*
arXiv:2405.13800, 2024a.
- 1074
- 1075 Yuan Yao, Tianyu Yu, Ao Zhang, Chongyi Wang, Junbo Cui, Hongji Zhu, Tianchi Cai, Haoyu Li,
1076 Weilin Zhao, Zhihui He, et al. Minicpm-v: A gpt-4v level mllm on your phone. *arXiv preprint*
1077 *arXiv:2408.01800*, 2024b.
- 1078
- 1079 Haoxuan You, Haotian Zhang, Zhe Gan, Xianzhi Du, Bowen Zhang, Zirui Wang, Liangliang Cao,
Shih-Fu Chang, and Yinfei Yang. Ferret: Refer and ground anything anywhere at any granularity.
arXiv preprint arXiv:2310.07704, 2023.

- 1080 Keen You, Haotian Zhang, Eldon Schoop, Floris Weers, Amanda Swearngin, Jeffrey Nichols, Yinfei
1081 Yang, and Zhe Gan. Ferret-ui: Grounded mobile ui understanding with multimodal llms. *arXiv*
1082 *preprint arXiv:2404.05719*, 2024.
- 1083 Peter Young, Alice Lai, Micah Hodosh, and Julia Hockenmaier. From image descriptions to visual
1084 denotations: New similarity metrics for semantic inference over event descriptions. *TACL*, 2014.
- 1085 Licheng Yu, Patrick Poirson, Shan Yang, Alexander C Berg, and Tamara L Berg. Modeling context
1086 in referring expressions. In *ECCV*, 2016.
- 1087
1088 Weihao Yu, Zhengyuan Yang, Linjie Li, Jianfeng Wang, Kevin Lin, Zicheng Liu, Xinchao Wang,
1089 and Lijuan Wang. Mm-vet: Evaluating large multimodal models for integrated capabilities. *arXiv*
1090 *preprint arXiv:2308.02490*, 2023.
- 1091 Zhou Yu, Dejing Xu, Jun Yu, Ting Yu, Zhou Zhao, Yueting Zhuang, and Dacheng Tao. ActivityNet-
1092 QA: A dataset for understanding complex web videos via question answering. In *AAAI*, 2019.
- 1093
1094 Yuqian Yuan, Wentong Li, Jian Liu, Dongqi Tang, Xinjie Luo, Chi Qin, Lei Zhang, and Jianke Zhu.
1095 Osprey: Pixel understanding with visual instruction tuning. In *CVPR*, 2024.
- 1096 Xiang Yue, Yuansheng Ni, Kai Zhang, Tianyu Zheng, Ruoqi Liu, Ge Zhang, Samuel Stevens,
1097 Dongfu Jiang, Weiming Ren, Yuxuan Sun, et al. Mmmu: A massive multi-discipline multimodal
1098 understanding and reasoning benchmark for expert agi. *arXiv preprint arXiv:2311.16502*, 2023a.
- 1099 Xiang Yue, Xingwei Qu, Ge Zhang, Yao Fu, Wenhao Huang, Huan Sun, Yu Su, and Wenhua Chen.
1100 Mammoth: Building math generalist models through hybrid instruction tuning. *arXiv preprint*
1101 *arXiv:2309.05653*, 2023b.
- 1102
1103 Yuhang Zang, Wei Li, Jun Han, Kaiyang Zhou, and Chen Change Loy. Contextual object detection
1104 with multimodal large language models. *arXiv preprint arXiv:2305.18279*, 2023.
- 1105
1106 Chi Zhang, Feng Gao, Baoxiong Jia, Yixin Zhu, and Song-Chun Zhu. Raven: A dataset for relational
1107 and analogical visual reasoning. In *CVPR*, 2019.
- 1108
1109 Haotian Zhang, Haoxuan You, Philipp Dufter, Bowen Zhang, Chen Chen, Hong-You Chen, Tsu-Jui
1110 Fu, William Yang Wang, Shih-Fu Chang, Zhe Gan, et al. Ferret-v2: An improved baseline for
1111 referring and grounding with large language models. *arXiv preprint arXiv:2404.07973*, 2024a.
- 1112
1113 Pan Zhang, Xiaoyi Dong, Yuhang Zang, Yuhang Cao, Rui Qian, Lin Chen, Qipeng Guo, Haodong
1114 Duan, Bin Wang, Linke Ouyang, et al. Internlm-xcomposer-2.5: A versatile large vision language
1115 model supporting long-contextual input and output. *arXiv preprint arXiv:2407.03320*, 2024b.
- 1116
1117 Ruohong Zhang, Liangke Gui, Zhiqing Sun, Yihao Feng, Keyang Xu, Yuanhan Zhang, Di Fu,
1118 Chunyuan Li, Alexander Hauptmann, Yonatan Bisk, et al. Direct preference optimization of video
1119 large multimodal models from language model reward. *arXiv preprint arXiv:2404.01258*, 2024c.
- 1120
1121 Shilong Zhang, Peize Sun, Shoufa Chen, Min Xiao, Wenqi Shao, Wenwei Zhang, Kai Chen, and
1122 Ping Luo. Gpt4roi: Instruction tuning large language model on region-of-interest. *arXiv preprint*
1123 *arXiv:2307.03601*, 2023.
- 1124
1125 Yi-Fan Zhang, Qingsong Wen, Chaoyou Fu, Xue Wang, Zhang Zhang, Liang Wang, and Rong
1126 Jin. Beyond llava-hd: Diving into high-resolution large multimodal models. *arXiv preprint*
1127 *arXiv:2406.08487*, 2024d.
- 1128
1129 Zicheng Zhang, Haoning Wu, Erli Zhang, Guangtao Zhai, and Weisi Lin. A benchmark for multi-
1130 modal foundation models on low-level vision: from single images to pairs. *arXiv preprint*
1131 *arXiv:2402.07116*, 2024e.
- 1132
1133 Yang Zhao, Zhijie Lin, Daquan Zhou, Zilong Huang, Jiashi Feng, and Bingyi Kang. Bubogpt:
Enabling visual grounding in multi-modal llms. *arXiv preprint arXiv:2307.08581*, 2023.
- Tianyu Zheng, Ge Zhang, Tianhao Shen, Xueling Liu, Bill Yuchen Lin, Jie Fu, Wenhua Chen, and
Xiang Yue. Opencodeinterpreter: Integrating code generation with execution and refinement. *arXiv*
preprint arXiv:2402.14658, 2024.

1134 Victor Zhong, Caiming Xiong, and Richard Socher. Seq2sql: Generating structured queries from
1135 natural language using reinforcement learning. *arXiv preprint arXiv:1709.00103*, 2017.
1136

1137 Baichuan Zhou, Ying Hu, Xi Weng, Junlong Jia, Jie Luo, Xien Liu, Ji Wu, and Lei Huang. Tinyllava:
1138 A framework of small-scale large multimodal models. *arXiv preprint arXiv:2402.14289*, 2024.

1139 Deyao Zhu, Jun Chen, Xiaoqian Shen, Xiang Li, and Mohamed Elhoseiny. Minigt-4: En-
1140 hancing vision-language understanding with advanced large language models. *arXiv preprint*
1141 *arXiv:2304.10592*, 2023.

1142 Fengbin Zhu, Wenqiang Lei, Youcheng Huang, Chao Wang, Shuo Zhang, Jiancheng Lv, Fuli Feng,
1143 and Tat-Seng Chua. TAT-QA: A question answering benchmark on a hybrid of tabular and textual
1144 content in finance. In *ACL*, 2021.

1145

1146 Yongshuo Zong, Ondrej Bohdal, and Timothy Hospedales. VI-icl bench: The devil in the details of
1147 benchmarking multimodal in-context learning. *arXiv preprint arXiv:2403.13164*, 2024.
1148
1149
1150
1151
1152
1153
1154
1155
1156
1157
1158
1159
1160
1161
1162
1163
1164
1165
1166
1167
1168
1169
1170
1171
1172
1173
1174
1175
1176
1177
1178
1179
1180
1181
1182
1183
1184
1185
1186
1187

A APPENDIX

A.1 RELATED WORK

Multimodal Large Language Models (MLLMs) (OpenAI, 2024; Islam & Moushi, 2024; Team et al., 2023; Li et al., 2024d; Huang et al., 2023) have recently emerged as a significant area of research focus. The development of MLLMs can be traced back to Frozen (Tsimpoukelli et al., 2021) and Flamingo (Alayrac et al., 2022; Awadalla et al., 2023), with more recent advancements such as LLaVA (Liu et al., 2023b) and MiniGPT-4 (Zhu et al., 2023) introducing the concept of visual instruction tuning. The past year has witnessed a boom of open-source MLLMs, some of which claim to rival GPT-4o on certain benchmarks. Notable examples include Emu2 (Sun et al., 2023b; 2024), VILA (Lin et al., 2024b), Idefics2/3 (Laurençon et al., 2024a; Laurençon et al., 2024a), Cambrian-1 (Tong et al., 2024a), InternLM-XComposer-2.5 (Dong et al., 2024a; Zhang et al., 2024b), InternVL2 (Chen et al., 2024c;b), MiniCPM-V (Yao et al., 2024b), CogVLM2 (Wang et al., 2023a; Hong et al., 2024a), BLIP-3 (Li et al., 2023d; Xue et al., 2024), LLaVA-OneVision (Li et al., 2024e), Llama3.1-V (Dubey et al., 2024), and the latest Qwen2-VL (Bai et al., 2023).

Research in MLLMs has expanded across several fronts: (i) scaling up the pre-training data (Lin et al., 2024b; McKinzie et al., 2024; Xue et al., 2024; Awadalla et al., 2024; Li et al., 2024j) and supervised instruction-tuning data (Hu et al., 2024b; Tang et al., 2024; Laurençon et al., 2024a; Tong et al., 2024a); (ii) enhancing high-resolution image comprehension (Lin et al., 2023b; Li et al., 2023i; Liu et al., 2024a; Dong et al., 2024a; Gao et al., 2024; Ge et al., 2024; Chen et al., 2024a; Zhang et al., 2024d; Xu et al., 2024c; Li et al., 2024l); (iii) exploring various vision encoders (Tong et al., 2024b; Shi et al., 2024) and vision-language connectors (Cha et al., 2024; Yao et al., 2024a; Li et al., 2024k; Cai et al., 2024); (iv) using mixture-of-experts (Lin et al., 2024a; Li et al., 2024g); (v) extending LLaVA-like architectures to region-level (Wang et al., 2023b; Zhao et al., 2023; Zang et al., 2023; Peng et al., 2023; Chen et al., 2023b; Zhang et al., 2023; You et al., 2023; Zhang et al., 2024a) and pixel-level (Lai et al., 2024; Rasheed et al., 2024; Yuan et al., 2024; Ren et al., 2024) understanding, multi-image reasoning (Jiang et al., 2024; Li et al., 2024e), UI comprehension (You et al., 2024; Hong et al., 2024b), and video understanding (Lin et al., 2023a; Xu et al., 2024a;b), among others.

Among the extensive body of literature on MLLMs, MM1.5 distinguishes itself as a significant upgrade over its predecessor, MM1 (McKinzie et al., 2024). The MM1.5 model family integrates a diverse set of core capabilities, including text-rich image understanding, visual referring and grounding, and multi-image reasoning. In contrast, recent general-purpose MLLMs such as Cambrian-1 (Tong et al., 2024a) and LLaVA-OneVision (Li et al., 2024e) have shown less satisfactory performance in handling referring and grounding tasks, and GPT-4o has to rely on set-of-mark (SoM) prompting (Yang et al., 2023) to understand image regions.

While several recent works have open-sourced detailed SFT data mixtures for public use (Laurençon et al., 2024a; Tong et al., 2024a), the precise impact of each data category and the best recipe to combine them remain under-explored. This is particularly true for models requiring diverse capabilities. MM1.5 stands out by providing a comprehensive empirical study that presents mature recipes for building performant MLLMs. The extension of MM1.5 to mobile UI understanding further enhances the uniqueness of this work.

Another emerging trend in the field is the development of lightweight MLLMs for potential edge deployment (Jin et al., 2024b; Huang et al., 2024; Beyer et al., 2024; Lu et al., 2024; Hinck et al., 2024; Li et al., 2024l; Zhou et al., 2024; He et al., 2024). In MM1.5, models with 1B and 3B parameters are offered, which outperform similar-sized models, such as Phi-3-Vision (Abdin et al., 2024b) and MiniCPM-V (Yao et al., 2024b).

A.2 PRE-TRAINING ABLATIONS

Beyond the SFT and continual pre-training, we emphasize the importance of large-scale, task-specific data used during pre-training in establishing robust foundations for models to effectively handle diverse tasks. For knowledge-heavy benchmarks like MMMU (Yue et al., 2023a), we found that model performance is highly sensitive to its text comprehension capabilities. The LLM’s ability to understand and process textual content is pivotal in addressing the complex reasoning and knowledge-representation challenges posed by these benchmarks, as also observed in Cambrian-1 (Tong et al., 2024a).

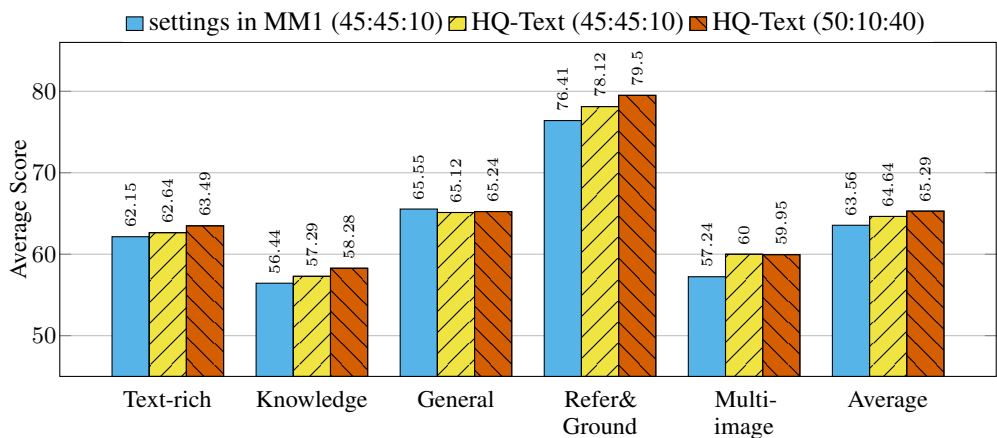


Figure 7: Performance comparison of all categories across different text-only data and pre-training data ratio. The figure highlights the performance improvement when replacing with *HQ-Text* data and the additional gains achieved by adjusting the ratio to 50:10:40. Note that the default setting for continual pre-training (OCR) and *All Mixture* for SFT are used for all models.

We incorporated a higher-quality and more diverse set of text-only datasets, referred to as *HQ-Text*, introduced by (Gunter et al., 2024), during the pre-training phase. These datasets were specifically curated to enhance the model’s language capabilities by providing deeper and more varied textual contexts, with a focus on general knowledge, mathematics, and coding. This update aims to strengthen the model’s ability in language-based reasoning.

As shown in Figure 7, by simply replacing with the new data, the average score on knowledge improves by 0.85 points.

In conjunction with the text-only datasets and the latest SFT recipes discussed in Section 2.2, we further refined our pre-training data composition. The original data ratio proposed in MM1 (McKinzie et al., 2024) was 45:45:10 for image-caption, interleaved image-text, and text-only data, respectively. Further experiments revealed that decreasing the amount of interleaved pre-training data and, respectively, increasing the weight of text-only data to a ratio of 50:10:40 resulted in improved performance across most tasks after SFT. We note that in contrast to pre-training ablations in MM1, for MM1.5, we conduct evaluations on downstream benchmarks post SFT to select our final pre-training mixture. We hypothesize that relying primarily on few-shot pre-training metrics may not be ideal, as the improvements on such evaluations may not effectively transfer to downstream performance. Our newly optimized data mix for MM1.5 not only enhances multimodal capabilities but also strengthens language understanding, leading to superior overall performance across benchmarks.

With the updated mixture, performance on text-rich average increased by 0.85, knowledge average by 0.99, and refer&ground tasks by around 1.4, as shown in Figure 7. Although there was a slight decrease of 0.05 on multi-image datasets due to the lower weighting of interleaved data, we consider this trade-off reasonable for maintaining strong performance across all tasks.

A.3 DETAILS OF SFT DATA FOR ABLATION & FINAL SFT MIXTURE

As presented in Table 5, we use a subset of our final SFT data when conducting the ablation study. The MM1.5 final mixture is presented in Figure 8.

A.4 MM1.5 BENCHMARK DETAILS

Benchmarks used for MM1.5 evaluation are summarized in Table 6, where for each *Category Average Score*, we directly calculate the average of each metric number within that capability category as follows, with detailed evaluation metrics listed in Table 6.

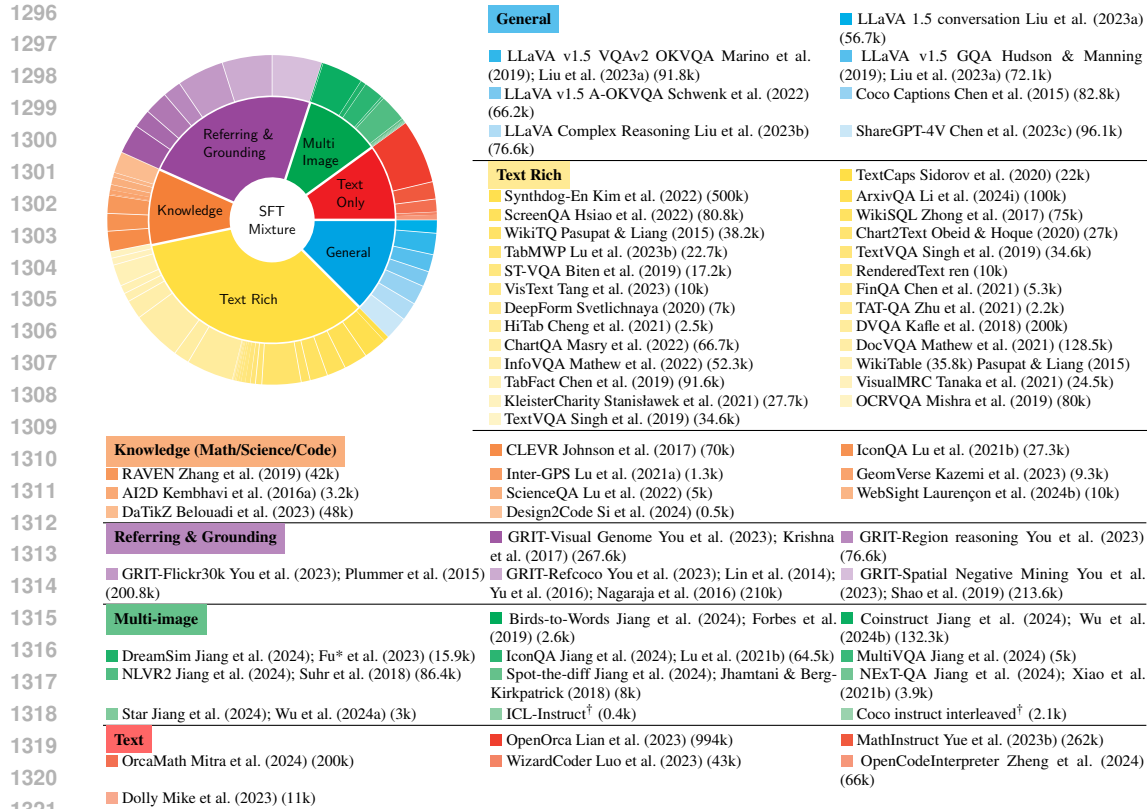


Figure 8: A high-quality data mixture used for MM1.5 supervised fine-tuning, including (i) single-image data for enhanced math/science reasoning, text-rich image understanding, and visual referring and grounding, (ii) multi-image data, and (iii) text-only data. (†) denotes in-house datasets with curation details in Appendix A.9.

Table 5: Overview of the SFT data used in ablation study.

Data category	Sub-category	Datasets	# QA
Single-image	General	LLaVA Complex Reasoning, LLaVA Conversation, ShareGPT-4v, Coco Caption, LLaVA v1.5 VQAv2 OKVQA, LLaVA v1.5 GQA, LLaVA v1.5 A-OKVQA	542K
	Text Rich	OCRVQA, Synthdog-En, TextCaps, TextVQA, DVQA, ChartQA, DocVQA, InfoVQA, VisualMRC, WikiTQ, DeepForm, KleisterCharity, TabFact	1.3M
	Refer&Ground	GRIT-Visual Genome, GRIT-Region reasoning, GRIT-Flickr30k, GRIT-Refcoco, GRIT-Spatial Negative Mining	1.08M
	Science	AI2D, ScienceQA	8K
	Math	GeomVerse, CLEVER, IconQA, RAVEN, Inter-GPS	150K
	Code	WebSight, DaTikZ, Design2Code	58K
Multi-image	-	DreamSim, NLVR2, Star, Birds-to-Words, IconQA, Spot-the-diff, ICL-instruct, Coinstruct, MultiVQA, NEXT-QA, Coco Instruct Interleaved	324K
Text-only	-	Dolly, OpenOrca, MathInstruct, WizardCoder, OrcaMath, OpenCodeInterpreter	1.71M

• **General Average Score:** average score of the corresponding metric scores from MME-Normalize³, Seed-IMG, POPE, LLaVA^W, MM-Vet and RealWorldQA.

• **Text-rich Average Score:** average score of the corresponding metric scores from WTQ, TabFact, OCRBench⁴, ChartQA⁵, TextVQA, DocVQA and InfoVQA.

³MME-Normalize is $(\text{MME-Perception} + \text{MME-Cognition})/2800 \times 100\%$.

⁴The accuracy of OCRbench is the total score normalized by $1000 \times 100\%$.

⁵Average of human part accuracy and augmented part accuracy.

Table 6: Details of benchmarks and their metrics used in MM1.5 ablation study. Benchmarks marked with (†) are excluded from the category average.

Category	Benchmark	Metric
General	MME Fu et al. (2024a)	Normalized Accuracy
	SEED Li et al. (2023b)	Seed-IMG
	POPE Li et al. (2023h)	Average of random, popular and adversarial
	LLaVA-Bench (Wild) Liu et al. (2023b)	GPT-assisted score
	MM-Vet Yu et al. (2023)	GPT-assisted score
	RealWorldQA x.ai	Accuracy
Text-rich	WTQ Pasupat & Liang (2015)	Accuracy
	TabFact Chen et al. (2019)	Accuracy
	OCRBench Liu et al. (2024b)	Accuracy
	ChartQA Masry et al. (2022)	Accuracy
	TextVQA Singh et al. (2019)	VQA Open Flamingo Accuracy
	DocVQA Mathew et al. (2021)	ANLS Score
	InfoVQA Mathew et al. (2022)	ANLS Score
Refer&Ground	Flickr30K Young et al. (2014)	Recall (IoU>0.5, any protocol)
	LVIS_Ferret Gupta et al. (2019); You et al. (2023)	Accuracy
	Refcoco Kazemzadeh et al. (2014)	Recall@1 (IoU>0.5)
	Refcoco+ Kazemzadeh et al. (2014)	Recall@1 (IoU>0.5)
	Refcocog Kazemzadeh et al. (2014)	Recall@1 (IoU>0.5)
	Ferret-Bench† You et al. (2023)	GPT-assisted score
Knowledge (Math/Science/Code)	AI2D Kembhavi et al. (2016b)	Accuracy
	ScienceQA Lu et al. (2022)	Accuracy-IMG
	MathVista Lu et al. (2023a)	GPT-assisted score
	MMMU Yue et al. (2023a)	Accuracy
Multi-image	Qbench2 Zhang et al. (2024e)	Accuracy
	Mantis Jiang et al. (2024)	Accuracy
	NLVR2 Suhr et al. (2018)	Accuracy
	BLINK Fu et al. (2024c)	Accuracy
	MVBench Li et al. (2023f)	Accuracy
	Muirbench† Wang et al. (2024)	Accuracy

- **Refer & ground Average Score:** average of the scores of Flickr30k, RefCOCO avg. and LVIS avg., where RefCOCO avg. is the average of RefCOCO A, RefCOCO B, RefCOCO+ A, RefCOCO+ B and RefCOCog, and LVIS avg. is the average of point and box metrics.
- **Knowledge Average Score:** average score of the corresponding metric scores from AI2D, ScienceQA, MathVista and MMMU.
- **Multi-image average score:** average of Qbench, Mantis, NLVR2, BLINK and MVBench metric scores.
- **MMBaseScore:** average score of the *General Average Score*, *Text-rich Average Score* and *Knowledge Average Score*. This aggregated metric is used in Section 2 to measure the impact of the general, text-rich, and knowledge capabilities of a model.

A.5 IMPACT OF SYNTHETIC CAPTIONS BY SELF-TRAINING

Besides using public captioning data mentioned in Section 2.3, we also follow (Fang et al., 2024) to study the effect of self-training using synthetic captions. This is particularly important because captioning data generated by black-box commercial models can sometimes be difficult to scale and data from open models, such as from the LLaVA-NeXT family may be constrained by these model’s inherent limitations. We develop a self-augmented image-caption data engine building on our previous work, MM1 (McKinzie et al., 2024) with a goal to provide high quality captions in a computationally efficient manner. Specifically, we fine-tune a pre-trained 3B MM1-style model on a mix of synthetic and approximately 8k human-annotated paragraph-length image captions (approximately 70 tokens on average). We then apply this captioner at scale to 290 million web-crawled images with resolutions ranging from 512 to 1024px. Following the approach in (Liu et al., 2024a), we perform concept filtering based on the generated captions, resulting in a dataset of 7 million high-quality captions, which includes numerous text-rich examples and alt-text-derived knowledge.

Building on this, we investigate the impact of the volume of synthetic caption data. The synthetic captions, ranging from 1.4 million to 7 million, show consistent improvements in model performance across various metrics, as illustrated in Figure 9. Specifically, a ratio of 0 on the x-axis indicates that no image-caption data is added to the original OCR dataset, while ratios ranging from 0.2 to 1.0 on the x-axis represent the proportion of the total 7M dataset included in the training. For example, a ratio of 0.2 corresponds to approximately 1.4M image-caption pairs added with the original OCR data while 1.0 denotes all 7M are added into training.

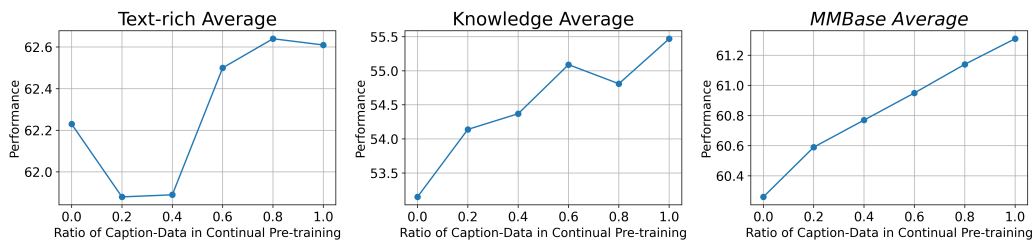


Figure 9: Impact of synthetic captions for continual pre-training the 3B model, building on top of the final MM1.5 strategy introduced in the main text, *i.e.*, including the OCR continual pre-training stage. We report the impact of adding incrementally more synthetic captions, up to 7M in total.

In contrast to the ShareGPT4V-PT and LLaVA-Recap-3M captions as explored in Section 2.3, we find that adding our in-house synthetic captions to the OCR data mixture can lead to consistent improvement for continual pre-training.⁶ We observe improvements in knowledge-related benchmarks and the aggregated *MMBase* scores that further scale with increased data volume. This is especially notable since our in-house captioner uses only a 3B model while LLaVA-Recap, for example, uses a 34B model for captioning.

Our results suggest that while a comparatively simple OCR mixture represents a strong baseline for continual pre-training data, high-quality captions can still lead to further improvements. However, the quality, distribution, perhaps even style and length of the generated captions seem crucial to realize gains. While our in-house captions empirically outperformed publicly available data in our specific setting, further research is necessary as to what, specifically, these improvements are attributable to and whether further improvements can be achieved. This investigation goes beyond the scope of this paper, and we aim to study synthetic captioning further in future work.

A.6 COMPARISON WITH SOTA MODELS

We compared our model with selected benchmarks in Section 3. Here, we present comparisons with more baselines on extensive benchmarks in Table 7 (Knowledge & General), 8 (Text-rich), Table 9 (Refer & s Ground), Table 10 (In-context Learning), and Table 11 (Multi-image).

⁶Experiments in this section are based on the final recipe from Section 3, with slightly different settings compared to those in Section A.2.

Table 7: Comparison with SOTA models on knowledge and general benchmarks. (†) The score is the summation of perception and cognition scores. Gemini-1.5-Pro, GPT-4V and GPT-4o numbers are from OpenVLM Leaderboard.

Model	Knowledge Benchmarks				General Benchmarks					
	A12D (test)	SQA (test)	MMMU (val)	MathV (testmini)	MME (P/C)	SEED [†]	POPE	LLaVA ^W	MM-Vet	RealWorldQA
<i>1B Model Comparison</i>										
LLaVAOneVision-0.5B Li et al. (2024c)	57.1	67.2	31.4	34.8	1238.0/240.0	65.5	–	–	29.1	55.6
SPHINX-Tiny Gao et al. (2024)	24.6	21.5	–	26.4	1261.2/242.1	–	82.2	52.3	23.8	–
DeepSeek-VL Lu et al. (2024)	–	–	32.2	31.1	–	–	87.6	–	34.8	–
TinyLLaVA Zhou et al. (2024)	–	60.1	–	–	–	–	86.1	60.8	25.8	–
Gemini Nano-1 Team et al. (2023)	37.9	–	26.3	27.3	–	–	–	–	–	–
IntenVL2-2B Chen et al. (2024b)	74.1	94.1	36.3	46.0	1864.3 [†]	70.9	85.2	60.0	39.7	57.4
MM1-1B McKinzie et al. (2024)	57.7	62.3	33.2	31.1	1393.2/217.1	65.6	87.4	67.5	39.4	51.2
MM1.5-1B	59.3	82.1	35.8	37.2	1365.7/245.7	70.2	88.1	71.6	37.4	53.3
MM1.5-1B-MoE	67.1	87.6	41.2	42.9	1511.9/361.1	71.4	88.6	75.5	39.8	57.8
<i>3B Model Comparison</i>										
MiniCPM-V 2.0-3B Yao et al. (2024b)	62.9	80.7	38.2	38.7	1808.2 [†]	67.1	87.8	69.2	38.2	55.8
VILA1.5-3B Lin et al. (2024b)	–	69.0	33.3	–	1442.4/–	67.9	85.9	–	–	–
TinyLLaVA Zhou et al. (2024)	–	69.1	–	–	1464.9/–	–	86.4	75.8	32.0	–
Gemini Nano-2 Team et al. (2023)	51.0	–	32.6	30.6	–	–	–	–	–	–
Bunny He et al. (2024)	–	78.3	41.4	–	1581.5/361.1	72.5	87.2	–	–	–
BLIP-3 Xue et al. (2024)	–	88.3	41.1	39.6	–	72.2	87.0	–	–	60.5
Phi-3-Vision-4B Abdin et al. (2024a)	76.7	90.8	40.4	44.5	1441.6/320.0	71.8	85.8	71.6	46.2	59.4
MM1-3B McKinzie et al. (2024)	62.4	69.4	33.9	32.0	1482.5/279.3	68.8	87.4	72.1	43.7	55.8
MM1.5-3B	65.7	85.8	37.1	44.4	1478.4/319.6	72.4	88.1	73.0	41.0	56.9
MM1.5-3B-MoE	69.9	89.8	42.9	46.9	1591.4/365.7	73.3	87.2	76.1	43.7	60.7
<i>7B Model Comparison</i>										
LLaVA-NeXT-7B Liu et al. (2024a)	–	70.1	35.8	34.6	1519.0/332.0	70.2	86.5	81.6	43.9	–
Idefics2-8B Laurençon et al. (2024a)	–	–	43.0	51.4	–	–	–	–	–	–
MM1-7B McKinzie et al. (2024)	66.0	72.6	37.0	35.9	1529.3/328.9	69.9	86.6	81.5	42.1	55.7
MM1.5-7B	72.2	89.6	41.8	47.6	1514.9/346.4	73.4	88.6	74.2	42.2	62.5
<i>30B Model Comparison</i>										
LLaVA-NeXT-34B Liu et al. (2024a)	–	81.8	51.1	46.5	1631.0/397.0	75.9	87.7	89.6	57.4	–
Cambrian-34B Tong et al. (2024a)	79.7	85.6	49.7	53.2	1689.3/–	75.3	–	–	–	67.8
MM1-30B McKinzie et al. (2024)	73.3	81.0	44.7	39.4	1637.6/431.4	72.1	87.6	89.3	48.7	59.4
MM1.5-30B	77.2	91.9	47.4	55.6	1646.2/405.7	75.0	88.6	80.4	52.0	69.0
Gemini-1.5-Pro Reid et al. (2024)	79.1	85.7	60.6	57.7	2110.6 [†]	–	88.2	95.3	64.0	64.1
GPT-4V OpenAI (2024)	75.9	82.1	53.8	48.7	1771.5 [†]	71.6	75.4	93.1	56.8	56.5
GPT-4o Islam & Moushi (2024)	84.6	90.7	69.2	61.3	2310.3 [†]	77.1	85.6	102.0	69.1	75.4

Table 8: Comparison with SOTA models on text-rich benchmarks. Numbers marked with (†) are obtained from Li et al. (2024c).

Model	Text-rich Benchmarks						
	WTQ (test)	TabFact (test)	OCRBench (test)	ChartQA (test)	TextVQA (val)	DocVQA (test)	InfoVQA (test)
<i>1B Model Comparison</i>							
LLaVOneVision-0.5B Li et al. (2024c)	–	–	–	61.4	–	70.0	41.8
SPHINX-Tiny Gao et al. (2024)	15.3	51.1	–	34.1	57.8	53.0	26.3
DeepSeek-VL Lu et al. (2024)	–	–	40.9	–	–	–	–
TinyLLaVA Zhou et al. (2024)	–	–	–	–	51.7	–	–
Gemini Nano-1 Team et al. (2023)	–	–	–	53.6	62.5	72.2	51.1
InternVL2-2B Chen et al. (2024b)	35.8	56.7	78.1	76.2	73.4	86.9	58.9
MM1-1B McKinzie et al. (2024)	19.9	49.8	56.6	61.8	68.2	68.4	38.5
MM1.5-1B	34.1	66.1	60.5	67.2	72.5	81.0	50.5
MM1.5-1B-MoE	38.9	71.4	62.6	73.7	76.1	84.8	55.9
<i>3B Model Comparison</i>							
MiniCPM-V 2.0-3B Yao et al. (2024b)	24.2	58.2	60.5	59.8	74.1	71.9	37.6
TinyLLaVA Zhou et al. (2024)	–	–	–	–	59.1	–	–
Gemini Nano-2 Team et al. (2023)	–	–	–	51.9	65.9	74.3	54.5
BLIP-3-4B Xue et al. (2024)	–	–	–	–	71.0	–	–
Phi-3-Vision-4B Abdin et al. (2024b)	47.4	67.8	63.7	81.4	70.1	83.3	49.0
MM1-3B McKinzie et al. (2024)	23.6	52.9	57.0	66.8	71.9	75.2	44.7
MM1.5-3B	41.8	72.9	65.7	74.2	76.5	87.7	58.5
MM1.5-3B-MoE	39.1	73.1	63.8	73.6	76.8	85.0	53.6
<i>7B Model Comparison</i>							
LLaVA-NeXT-7B Liu et al. (2024a)	–	–	–	–	64.9	–	–
Idefics2-8B Laurençon et al. (2024a)	–	–	–	–	73.0	74.0	–
DocOwl-1.5-Chat Hu et al. (2024a)	40.6	80.2	–	70.2	68.6	82.2	50.7
MM1-7B McKinzie et al. (2024)	28.8	55.5	62.6	72.6	72.80	76.8	45.5
MM1.5-7B	46.0	75.9	63.5	78.6	76.5	88.1	59.5
<i>30B Model Comparison</i>							
LLaVA-NeXT-34B Liu et al. (2024a)	–	–	–	–	69.5	–	–
Cambrian-34B Tong et al. (2024a)	–	–	60.0	75.6	76.7	75.5	–
MM1-30B McKinzie et al. (2024)	33.3	58.9	60.6	76.9	73.5	75.8	47.3
MM1.5-30B	54.1	84.0	65.8	83.6	79.2	91.4	67.3
Gemini-1.5-Pro Reid et al. (2024)	–	–	75.4	87.2	78.7	93.1	81.0
GPT-4V OpenAI (2024)	–	–	64.5	78.5 [†]	–	88.4 [†]	–
GPT-4o Islam & Moushi (2024)	–	–	73.6	85.7 [†]	–	92.8 [†]	–

Model	Refer and Ground Benchmarks					
	RefCOCO (testA/B)	RefCOCO+ (testA/B)	RefCOCog (test)	Flickr30k (test)	LVIS-Ref (box/point)	Ferret-Bench (avg.)
<i>1B Model Comparison</i>						
SPHINX-Tiny Gao et al. (2024)	86.9/77.9	78.5/63.7	78.9	–	–	–
MM1-1B McKinzie et al. (2024)	0/0	0/0	0	0	51.4/51.6	47.3
MM1.5-1B	89.3/81.9	83.7/69.3	82.8	83.0	69.7/54.7	67.4
MM1.5-1B-MoE	91.0/84.8	86.0/73.0	84.7	85.4	71.4/56.7	69.6
<i>3B Model Comparison</i>						
MiniCPM-v2-3B Yao et al. (2024b)	–	–	–	–	48.2/47.7	22.1
Phi-3-Vision-4B Abdin et al. (2024b)	46.3 / 36.1	42.0 / 28.8	37.6	27.12	53.8/54.5	32.2
InternVL2 Chen et al. (2024b)	88.2 / 75.9	82.8 / 63.3	78.3	51.6	51.0 / 51.1	35.0
MM1-3B McKinzie et al. (2024)	0/0	0/0	0	0	52.9/53.9	46.3
MM1.5-3B	92.0/86.1	87.7/75.9	86.4	85.9	76.3/59.5	69.5
MM1.5-3B-MoE	92.6/86.4	88.0/77.8	86.4	85.8	79.3/54.5	72.2
<i>7B Model Comparison</i>						
Qwen-VL-7B Bai et al. (2023)	92.3/84.5	88.6/76.8	86.3	–	–	–
MiniGPT-v2-7B Chen et al. (2023a)	91.3/84.3	85.5/73.3	84.3	–	–	–
LLaVA-OneVision-7B Abdin et al. (2024b)	80.0/61.6	76.9/56.2	70.0	50.1	51.2/51.4	38.4
Ferret-7B You et al. (2023)	91.4/82.5	87.4/73.1	84.8	82.2	79.4/67.9	64.5
Ferret-V2-7B Zhang et al. (2024a)	94.7/88.7	92.8/79.3	89.3	85.8	86.6/74.6	75.6
MM1-7B McKinzie et al. (2024)	0/0	0/0	0	0	53.1/53.3	48.5
MM1.5-7B	92.5/86.7	88.7/77.8	87.1	85.3	79.4/53.4	72.6
<i>Larger (>13B) Model Comparison</i>						
Ferret-13B You et al. (2023)	92.4/84.4	88.1/75.2	86.3	84.8	80.5/68.4	66.3
Ferret-V2-13B Zhang et al. (2024a)	95.0/88.9	92.8/81.4	90.0	86.3	87.7/75.1	74.9
MM1-30B McKinzie et al. (2024)	0/0	0/0	0	0	53.4/52.7	50.9
MM1.5-30B	94.9/89.5	92.4/83.5	90.0	87.5	84.9/61.4	77.1

Table 10: Comparison with SOTA models on VL-ICL benchmark Zong et al. (2024) for multimodal in-context learning. 4-shot accuracy reported for each subtask.

Model	VL-ICL Benchmark						
	CLEVR	Matching MiniImageNet	Open MiniImageNet	Operator induction	Operator induction interleaved	TextOCR	Avg.
<i>1B Model Comparison</i>							
MM1-1B McKinzie et al. (2024)	25.0	49.3	73.0	16.7	8.3	33.5	34.3
MM1.5-1B	39.0	52.0	84.0	60.0	36.7	34.0	51.0
MM1.5-1B-MoE	33.0	56.5	89.0	56.7	56.7	44.0	56.0
<i>3B Model Comparison</i>							
Phi-3-Vision-4B Abdin et al. (2024b)	17.0	50.0	1.0	26.7	8.3	14.0	19.5
MM1-3B McKinzie et al. (2024)	27.5	50.0	79.0	18.3	13.3	34.0	37.0
MM1.5-3B	33.5	59.0	88.0	48.3	66.7	42.5	56.3
MM1.5-3B-MoE	32.0	58.0	92.0	63.3	65.0	47.5	59.6
<i>7B Model Comparison</i>							
OpenFlamingo-9B Awadalla et al. (2023)	18.8	50.0	51.2	2.8	2.8	0.0	20.9
Idefics-9B Laurençon et al. (2024b)	27.7	50.0	53.8	7.8	6.1	22.8	28.0
Otter-9B Li et al. (2023a)	8.2	50.4	28.5	12.2	7.2	0.8	17.9
InternLM-XComposer2-7B Dong et al. (2024a)	20.0	50.1	49.0	39.4	11.1	16.0	30.9
Qwen-VL-Chat-7B Bai et al. (2023)	26.8	56.4	58.0	18.9	8.9	22.3	31.9
LLaVA-NeXT-7B Liu et al. (2024a)	17.8	50.0	0.0	3.3	5.0	0.0	12.7
MM1-7B McKinzie et al. (2024)	33.0	69.5	97.5	40.0	45.0	32.0	52.8
MM1.5-7B	25.5	52.8	98.5	68.3	60.0	31.0	56.0
<i>Larger (>30B) Model Comparison</i>							
Idefics-80B- Laurençon et al. (2024b)	31.5	50.0	52.5	21.7	28.3	29.5	35.6
Emu2-Chat-37B Sun et al. (2023a)	14.8	50.0	28.2	21.7	10.0	36.5	26.9
MM1-30B McKinzie et al. (2024)	25.0	63.0	98.5	51.7	38.3	36.0	52.1
MM1.5-30B	46.5	66.5	100.0	65.0	80.0	44.5	77.6
GPT-4V OpenAI (2024)	42.0	81.0	56.0	92.0	74.0	50.0	65.8

Table 11: Comparison with SOTA models on multi-image benchmarks. The result with mark (†) in the row of GPT-4V is from GPT-4o. MVBench Li et al. (2024h) is treated as a multi-image benchmark to test the zero-shot transfer capability of MM1.5 to video understanding tasks.

Model	Multi-image Benchmarks					
	QBench2 (val)	Mantis (test)	NLVR2 (val)	MVBench	BLINK (val)	Muirbench (test)
<i>1B Model Comparison</i>						
LLaVA-NeXT-Interleave-0.5B Li et al. (2024f)	52.0	45.6	67.8	45.6	39.2	–
LLaVAOneVision-0.5B Li et al. (2024c)	48.8	39.6	63.4	45.5	52.1	25.5
MM1-1B McKinzie et al. (2024)	43.4	41.5	50.9	43.8	40.3	30.7
MM1.5-1B	66.4	50.7	79.0	45.8	46.3	34.7
MM1.5-1B-MoE	70.9	51.2	83.2	48.3	43.7	40.9
<i>3B Model Comparison</i>						
BLIP-3-4B Xue et al. (2024)	75.1	56.7	–	–	49.7	–
Phi-3-Vision-4B Abdin et al. (2024b)	56.8	47.9	53.6	46.7	44.2	38.0
MM1-3B McKinzie et al. (2024)	41.4	45.2	51.7	44.8	41.5	28.0
MM1.5-3B	73.2	54.8	83.8	47.7	46.8	44.3
MM1.5-3B-MoE	73.8	54.4	86.0	50.3	49.8	45.6
<i>7B Model Comparison</i>						
LLaVA-v1.5-7B Liu et al. (2023a)	49.3	31.3	53.9	36.0	37.1	23.5
LLaVA-NeXT-Interleave-7B Li et al. (2024f)	74.2	62.7	88.8	53.1	52.6	38.9
Idefics2-8B Laurençon et al. (2024a)	57.0	48.9	86.9	29.7	45.2	26.1
Mantis-Idefics2-8B Jiang et al. (2024)	75.2	57.1	89.7	51.4	49.1	44.5
MM1-7B McKinzie et al. (2024)	43.6	51.6	59.9	45.3	40.0	30.4
MM1.5-7B	73.2	57.6	86.9	48.3	48.2	49.1
<i>Larger (>14B) Model Comparison</i>						
LLaVA-NeXT-Interleave-14B Li et al. (2024f)	76.7	66.4	91.1	54.9	52.1	–
Emu2-Chat-37B Sun et al. (2023a)	50.1	37.8	58.2	39.7	36.2	33.6
MM1-30B McKinzie et al. (2024)	42.8	52.5	63.1	47.1	43.5	36.7
MM1.5-30B	79.3	64.6	90.6	54.0	50.2	58.2
GPT-4V OpenAI (2024)	76.5	62.7	88.8	43.5	51.1	68.0 [†]

1620 A.7 MM1.5-VIDEO

1621
1622 The multi-image reasoning capability shown in MM1.5 naturally leads us to develop **MM1.5-Video**
1623 for video understanding. It takes a video and an instruction as input and generates the response.
1624 For the inputs, we uniformly sample N frames from the video at an arbitrary length and feed them
1625 into the model as multi-image inputs without special frame assembly. Due to the token limits, we
1626 disable the dynamic image splitting for each frame, and the vision encoder generates the feature maps
1627 frame-by-frame independently. Specifically, we sample 24 frames for each video, and each frame is
1628 represented by 144 tokens.

1629 We introduce two variants for MM1.5-Video. First, we build MM1.5-Video as a *training-free* model,
1630 which is achieved by directly adopting the pre-trained MM1.5 image models to video tasks without
1631 being fine-tuned on any video data. This saves a lot of computation resources and demonstrates
1632 MM1.5’s capability of transferring knowledge to new domains.

1633 Second, we introduce the *supervised fine-tuning (SFT)* model where we fine-tune MM1.5 image
1634 models on video instruction-tuning datasets to improve its temporal modeling capability for video
1635 tasks. We use a mixture of public video datasets from ShareGPTVideo (Zhang et al., 2024c) (556K),
1636 VideoChat2 (Li et al., 2023e) (225K), and ActivityNet-QA (Yu et al., 2019) (31.5K). These datasets
1637 contain a variety of videos types, spanning different tasks (e.g., open-ended and multiple choice
1638 questions), viewpoints (e.g., first- and third-person views), and lengths (e.g., videos from a few
1639 seconds to tens of minutes).

1640 A.7.1 BENCHMARKS AND METRICS

1641 We compare our video training-free and SFT models with state-of-the-art methods on multiple video
1642 question-answering (VideoQA) tasks and benchmarks.

1643 **Open-Ended Benchmarks** evaluate the performance of a model to answer questions in a free-form
1644 style. For this task, we include ActivityNet-QA (Yu et al., 2019) and VCGBench (Maaz et al., 2024).
1645 Following prior work (Xu et al., 2024b), we use GPT-3.5-Turbo-0125 to assess the accuracy
1646 and score for the prediction. Considering that the labeled answers of these two datasets are typically
1647 short (e.g., one word or phrase), we also evaluate on the LLaVA-Hound (Zhang et al., 2024c), which
1648 requires the model to generate more detailed answers. This is useful for assessing performance on
1649 tasks involving detailed video understanding. We follow their original setting to report the score from
1650 GPT-3.5-Turbo-0301 and consider a score value ≥ 3 as correct for accuracy calculation.

1651 **Multiple Choice Benchmarks** require the model to pick the correct answer from multiple choices.
1652 For this evaluation, we include VideoMME (Fu et al., 2024b), EgoSchema (Mangalam et al., 2024),
1653 NEXTQA (Xiao et al., 2021a), and IntentQA (Li et al., 2023c). VideoMME is a comprehensive
1654 evaluation dataset containing video from a few seconds to one hour in length. EgoSchema consists of
1655 egocentric videos and involves complex long-form temporal understanding and reasoning. NEXTQA
1656 and IntentQA are collected from the same video source, but IntentQA focuses on predicting intents in
1657 daily social activities. For all these datasets, the accuracy of selecting the correct answer from the
1658 options is used as the evaluation metric.

1660 A.7.2 RESULTS

1661 **Training-free results** are shown in Table 12 and 13. MM1.5-Video demonstrates greater capability on
1662 Multiple Choice VideoQA, where MM1.5-Video-3B already outperforms state-of-the-art training-free
1663 7B models on all benchmarks. We also find that MM1.5-Video can follow the instruction to precisely
1664 output the predicted option; however, most existing methods (Li et al., 2024h) use structured answer
1665 prompts (e.g., "Best Option: (") to guide their models to generate answers in a desirable format.
1666 On the other hand, MM1.5-Video achieves only on-par performance compared to SlowFast-LLaVA
1667 on the open-ended benchmarks. We hypothesize that this is because our multi-image SFT datasets
1668 contain primarily multiple choice tasks, making such a task formulation most similar to the training
1669 data.

1670 **SFT results** are also shown in Table 12 and 13. First, we observe that fine-tuning MM1.5-Video on
1671 video datasets can improve its performance on all tasks. Second, on both open-ended and multiple
1672 choice benchmarks, our small model, MM1.5-Video-1B, significantly outperforms LLaVAOneVision-

Table 12: Comparison with SOTA models on Open-Ended and Multiple Choice benchmarks.

Model	Video Data	Open-Ended Benchmarks		Multiple Choice Benchmarks			
		ActivityNet-QA (test)	VCGBench (test)	VideoMME (w/o subs)	EgoSchema (subset)	NExTQA (val)	IntentQA (val)
<i>Training-Free Model Comparison</i>							
DeepStack-L-7B Meng et al. (2024)	✗	49.3	–	–	38.4	61.0	–
IG-VLM-7B (LLaVA-v1.6) Kim et al. (2024)	✗	54.3	3.03	–	35.8	63.1	60.3
SlowFast-LLaVA-7B Xu et al. (2024b)	✗	55.5	3.04	40.7	47.2	64.2	60.1
MM1.5-Video-1B (Training-free)	✗	46.8	2.86	45.6	45.4	70.0	67.8
MM1.5-Video-3B (Training-free)	✗	50.9	3.04	48.4	48.4	72.8	72.7
MM1.5-Video-7B (Training-free)	✗	52.5	3.05	52.4	49.6	76.1	76.7
<i>SFT Model Comparison</i>							
VideoChatGPT-7B Maaz et al. (2024)	✓	35.2	2.42	–	–	–	–
Video-LLaVA-7B Lin et al. (2023a)	✓	45.3	2.84	39.9	–	–	–
Vista-LLaMA-7B Ma et al. (2024)	✓	48.3	–	–	–	60.7	–
MovieChat+7B Song et al. (2024)	✓	48.1	–	–	–	54.8	–
VideoChat2-7B Li et al. (2024h)	✓	49.1	2.98	–	–	68.6	81.9
Video-LLaMA2-7B Cheng et al. (2024)	✓	50.2	3.13	47.9	51.7	–	–
PLLaVA-7B Xu et al. (2024a)	✓	56.3	–	–	–	–	–
LLaVA-NeXT-Interleave-0.5B Li et al. (2024f)	✓	48.0	3.07	–	–	59.5	–
LLaVA-NeXT-Interleave-7B Li et al. (2024f)	✓	55.3	3.42	–	–	78.2	–
LLaVAOneVision-0.5B Li et al. (2024c)	✓	50.5	3.12	44.0	26.8	57.2	–
LLaVAOneVision-7B Li et al. (2024c)	✓	56.6	3.51	58.2	60.1	79.4	–
MM1.5-Video-1B (SFT)	✓	56.1	3.14	45.7	51.0	71.8	74.2
MM1.5-Video-3B (SFT)	✓	57.9	3.17	49.5	52.4	74.7	81.2
MM1.5-Video-7B (SFT)	✓	60.9	3.22	53.5	57.2	76.9	86.6

Table 13: Comparison with SOTA models on LLaVA-Hound benchmarks. (†) indicates the published version released at <https://huggingface.co/ShareGPTVideo/LLaVA-Hound-SFT>.

Model	In-domain Benchmarks			Out-of-domain Benchmarks			
	ActivityNet-QA	VIDAL-QA	WebVid-QA	MSVD-QA	MSRVTT-QA	TGIF-QA	SSV2-QA
Video-ChatGPT-7B Maaz et al. (2024)	34.2	29.4	38.9	34.1	25.7	31.4	19.4
LLaMA-VID-7B Li et al. (2023g)	36.5	30.6	37.0	34.1	25.0	27.2	22.2
Chat-UniVi-7B Jin et al. (2024a)	39.4	31.4	40.1	35.6	25.9	33.2	20.6
Video-LLaVA-7B Lin et al. (2023a)	41.4	34.3	42.5	39.5	30.8	33.0	24.3
LLaVA-HOUND-SFT-7B†	62.8	56.3	66.8	62.2	52.6	61.1	35.4
MM1.5-Video-1B (Training-free)	49.0	42.6	55.8	49.8	43.3	47.6	27.2
MM1.5-Video-3B (Training-free)	51.5	45.4	58.5	51.1	46.0	49.2	28.2
MM1.5-Video-7B (Training-free)	52.8	48.7	58.5	52.9	48.1	49.8	30.4
MM1.5-Video-1B (SFT)	65.7	60.6	68.7	65.0	55.3	64.0	34.0
MM1.5-Video-3B (SFT)	67.8	63.4	71.1	65.2	57.2	64.9	35.2
MM1.5-Video-7B (SFT)	68.5	68.5	71.5	67.2	59.3	65.5	37.9

0.5B (*e.g.*, 24.2% on EgoSchema and 14.6% on NExTQA) and achieves the state-of-the-art results. Third, our 7B model achieves state-of-the-art performance on ActivityNet-QA (*e.g.*, outperforming LLaVAOneVision-7B by 4.3%) and very strong results (mostly runner-up) on other benchmarks by using only public video datasets. We are impressed by the superior results of LLaVAOneVision-7B, especially on long-form video benchmarks such as VideoMME and EgoSchema. We hypothesize this can be due to that (i) it is trained on their re-annotated video datasets with better labeling quality, (ii) it takes more video frames as inputs (*i.e.*, 32 vs. 24), (iii) it uses multiple training stages on joint image and video datasets. We will explore these directions to improve our model in future work. Lastly, MM1.5-Video achieves state-of-the-art performance on the LLaVA-Hound benchmarks, which demonstrates our capability for detailed video understanding.

A.8 MM1.5-UI

One of the most promising applications of MLLMs that has recently gained popularity is using them to understand and act on user interfaces (UIs) on behalf or alongside users (Hong et al., 2024b; Baechler et al., 2024; You et al., 2024; Li & Li, 2023), which could significantly boost users’ productivity and efficiency when interacting with digital devices. This application typically involves providing a model input of: (i) an image of the graphical user interface (GUI) of a device (*i.e.*, phone or computer) screen; and (ii) instructions on either knowledge *grounded* on certain areas or the entirety of the screen (*e.g.*, Is this element at $\langle x1, x2, y1, y2 \rangle$ clickable?), or asking it to *refer* to certain areas of the screen that fit the questions’ criterion (*e.g.*, Where is the text ‘login’ on the screen?). Beyond referring and grounding abilities, excelling on UI tasks also requires text-rich image understanding ability to

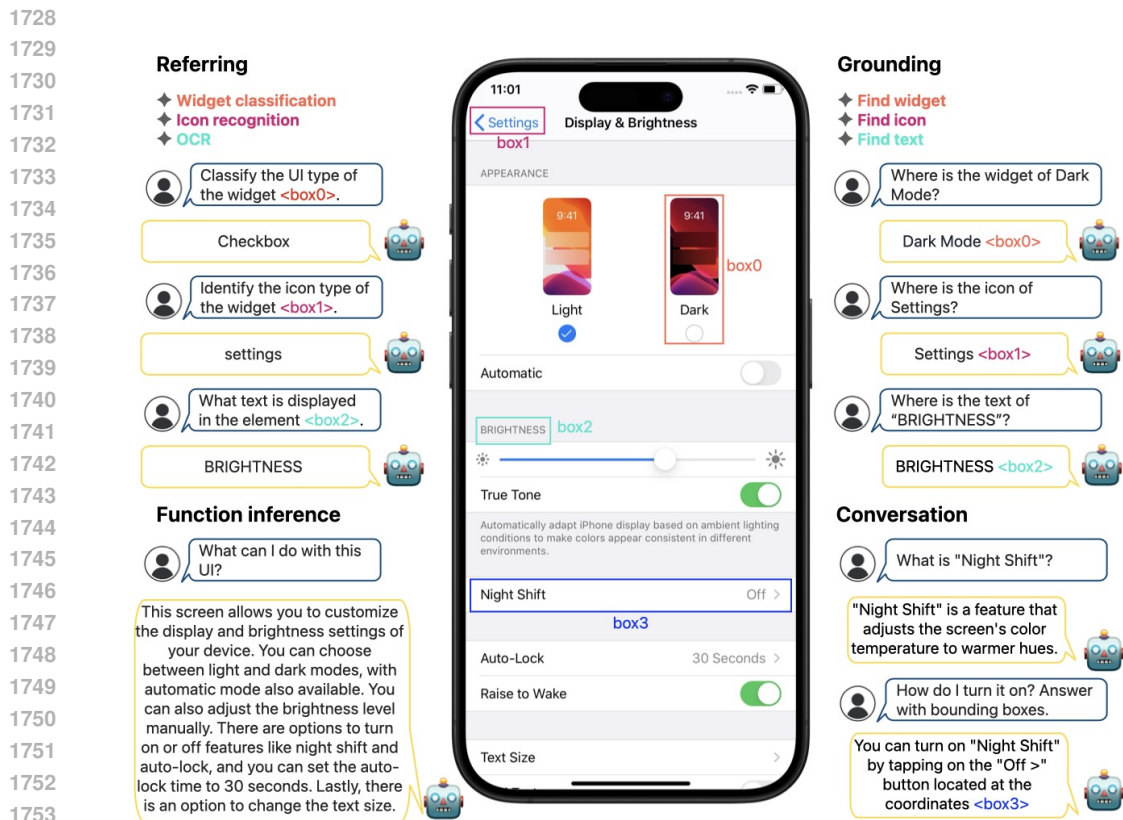


Figure 10: Illustration of the UI understanding capability shown in MM1.5-UI. Our single model is able to perform a variety of referring and grounding tasks and establish new state-of-the-arts. Moreover, it can summarize the functions of the UI screen and engage with users through conversations.

understand text-dense UIs, and background knowledge about typical user interactions on devices, which makes MM1.5 a perfect candidate to be developed into a highly capable UI understanding model.

Towards this goal, we developed **MM1.5-UI**, an MM1.5 model variant further fine-tuned specifically on UI data that achieves competitive performance on UI understanding tasks and establishes new state-of-the-art performance in various benchmarks. Figure 10 illustrates a single MM1.5-UI model’s wide range of UI understanding capabilities on an iPhone screenshot. The model can find certain text (“BRIGHTNESS”) on the left side (box2), correctly identify the settings icon at the top left (box1), classify a UI element on the right as a checkbox (box0), and maintain a multi-turn conversation about the “Night Shift” function (box3) in the UI.

A.8.1 BENCHMARKS AND METRICS

We train and evaluate MM1.5-UI on a variety of public and elementary UI understanding tasks used in Ferret-UI (You et al., 2024). These tasks are established benchmarks in literature that cover multiple aspects of UI understanding, and allow us to fairly compare MM1.5-UI against prior work:

- **Public Benchmarks** include screen2words (Wang et al., 2021): a screen-level captioning task; widget captions (Li et al., 2020): a widget-level captioning task; and taperception (Schoop et al., 2022): predicting the tapability of a certain widget on the UI.
- **Ferret-UI** elementary tasks are split into two categories: Grounding (Grd-*) are questions querying for a certain area on the screen, such as finding an icon; and Referring (Ref-*) are questions given a certain area on the screen, such as recognizing text within a screen area (*i.e.*, OCR). Each of these tasks also has an iOS (*-i) and Android (*-A) version, forming four categories of tasks (*e.g.*, Grounding task on Android is Grd-A).

Table 14: Comparison with SOTA models on UI benchmarks. S2W: screen2words, WiC: widget captioning, TaP: taperception. (†) denotes per-task fine-tuning. 1 ep. means 1 epoch model training.

Model	Public Benchmarks			Ferret-UI Elementary Tasks			
	S2W	WiC	TaP	Ref-i	Ref-A	Grd-i	Grd-A
Spotlight Li & Li (2023)	106.7	141.8	88.4	-	-	-	-
PaliGemma-3B† Beyer et al. (2024)	119.6	148.4	-	-	-	-	-
Ferret-UI-13B You et al. (2024)	113.4	142.0	78.4	80.5	82.4	79.4	83.5
MM1.5-UI-1B	103.0	144.4	79.3	90.0	88.6	86.5	88.2
MM1.5-UI-3B	103.3	145.0	80.4	90.8	89.2	87.3	88.8
MM1.5-UI-7B	100.6	149.7	80.3	91.2	89.2	87.2	88.6
MM1.5-UI-30B	106.0	145.9	80.6	91.8	89.7	88.2	89.1
<i>Ablation on MM1.5 SFT on UI tasks</i>							
MM1.5-UI-3B (1 ep.)	103.9	145.2	77.4	88.6	87.7	86.0	87.9
MM1.5-UI-3B (1 ep., w/o MM1.5 SFT)	103.8	139.5	75.3	88.2	87.4	85.5	87.1

More details of the benchmarks can be found in Appendix A.10 and the original Ferret-UI paper (You et al., 2024).

A.8.2 RESULTS

MM1.5-UI models are trained by further fine-tuning the final MM1.5 models on the Ferret-UI data mixture (You et al., 2024), which includes training data corresponding to the above elementary UI tasks and additional GPT-4-generated conversations about functionalities and descriptions about the UIs’ functionality and layouts. There are 801K samples in total. All models are trained with the same batch size and learning rate as the original MM1.5 model.

Comparison with Prior Art. Results are summarized in Table 14. Our MM1.5-UI models outperform prior best models in nearly all benchmarks except Screen2words. In particular, even our 1B model is able to outperform the Ferret-UI model in its proposed elementary tasks by a wide margin despite being ten times smaller. The performance difference is most significant on iOS tasks at 9.1 points on average. This demonstrates that the abilities learned by MM1.5 are relevant and useful for UI tasks.

When comparing the performance across individual benchmarks, MM1.5-UI demonstrates a clear hierarchy of difficulties among tasks that focus on different types of UI elements, similar to Ferret-UI (You et al., 2024). Tasks focused on text are the most challenging, followed by those involving icons, while widget-based tasks are the easiest. This trend holds for both referring and grounding tasks. However, MM1.5-UI shows a notable performance improvement in icon-based tasks, significantly narrowing the gap between icon and widget tasks. Ferret-UI highlighted the importance of resolution for tasks involving smaller elements like icons. The higher resolution and dynamic image splitting used in MM1.5-UI further confirm that resolution is particularly beneficial for enhancing performance in icon-related tasks.

Impact of MM1.5 SFT on UI tasks. To highlight the effectiveness of the MM1.5 SFT mixture on downstream UI tasks (*i.e.*, in MM1.5-UI), we compare the performance of the full MM1.5-UI model with a baseline UI model fine-tuned with UI data on the pre-training checkpoint that MM1.5 was trained on. Both models are trained for one epoch using the Ferret-UI dataset, and their results are presented in Table 14. The final MM1.5-UI model, which underwent SFT for general domain, text-rich, and refer&ground tasks, achieves superior UI performance within the same number of training steps. This demonstrates the strong transfer capability of MM1.5 for UI applications and contributes to its performance improvement over prior SOTA models.

Impact of model scaling. We observe overall performance improvements as models scale, though gains in all metrics remain modest, suggesting that larger models may be constrained by factors such as data diversity, image resolution, or overfitting. For instance, in the most challenging OCR tasks, 47.8% of incorrect responses contain the ground truth as a strict substring of the generated response, or vice versa. This suggests the model accurately recognized the text but failed to trim or include the correct amount. Additionally, the performance of the 7B and 30B models appears to have plateaued,

1836 indicating that larger, more diverse datasets and joint SFT of UI and core capabilities could further
1837 improve the performance.
1838

1839 A.9 MM1.5 IN-HOUSE MULTI-IMAGE SFT DATA 1840

1841 We generated two sets of in-house SFT data for the multi-image capabilities of our model: coco-
1842 instruct-interleaved and icl-instruct.

1843 Coco-instruct-interleaved was generated using an LLaVa-style approach using our text-only LLM.
1844 We input COCO image captions for two images, along with a prompt requiring the LLM to generate
1845 a conversation between a user and an assistant, with the two images inserted in context. This dataset
1846 helps our model learn conversational multi-image capabilities. An example from this dataset is shown
1847 below. This dataset contains ~2k examples, with 2 images per example.

1848 **User:** <image 1> What do you see in the following picture?

1849 **Assistant:** I see an open beige toilet with a monitoring device attached to the
1850 seat. The device appears to be displaying various metrics, such as temperature and
1851 pressure, and it is likely used for medical purposes.

1852 **User:** <image 2> What about this picture?

1853 **Assistant:** I see a row of parking meters sitting next to each other near a street.
1854 The meters are typical of those used to enforce parking regulations in many cities.

1855 **User:** What is the difference between the two pictures?

1856 **Assistant:** The first picture depicts a toilet with a monitoring device, while the
1857 second picture shows a row of parking meters. These are two very different objects
1858 in different settings. The first picture is likely used for medical purposes, while the
1859 second picture is used to regulate parking in cities.

1860 Icl-instruct was generated manually to help the model retain in-context learning abilities from pre-
1861 training along with more nuanced in-context learning tasks that require multi-step reasoning from
1862 the model. This dataset contains different varieties of in-context learning tasks, some of which are
1863 similar to those found in the VL-ICL benchmark (Zong et al., 2024). We found that including this
1864 dataset, which contains ~500 examples, greatly boosts the models' in-context learning performance.
1865

1866 A.10 MM1.5-UI BENCHMARK DETAILS 1867

1868 The public benchmark tasks and metrics for evaluating MM1.5-UI are:

- 1869 • **Screen2words** is a captioning task where each complete screen is paired with 5 ground-truth
1870 high-level summaries under ten words. The generated summaries' quality is measured by CIDEr
1871 score between the ground-truth and generated summaries.
- 1872 • **Widget Captioning** is a captioning task where a certain screen area that corresponds to a widget
1873 (e.g., button, list item) is paired with 3 ground-truth captions. The generated summaries' quality is
1874 measured by CIDEr score similar to Screen2words.
- 1875 • **Tapereception** is a binary classification task where a certain screen area that correspond to a widget
1876 (e.g., button, list item) is paired with a ground-truth binary label of whether the screen area is
1877 'tappable' (i.e., clickable by users). The generated labels' quality is measured by F1 score.
1878

1879 The Ferret-UI Elementary task benchmarks used to evaluate MM1.5-UI, organized by capability
1880 categories, are:

- 1881 • **Ferret-UI Grounding (Grd-i/A)** is a set of three grounding-based UI tasks introduced in Ferret-
1882 UI (You et al., 2024). These tasks query for certain areas of screens that meet certain criteria. They
1883 include finding a widget given a text description, finding an icon given the class of the icon, and
1884 finding a text location on screen. The expected response from the model is a bounding box, and the
1885 quality of the bounding box is measured by Recall with IoU>0.5.
- 1886 • **Ferret-UI Referring (Ref-i/A)** is a set of three referring-based UI tasks introduced in Ferret-
1887 UI (You et al., 2024). These tasks query about knowledge or characteristics that correspond to
1888 certain areas of the screens. They include classifying the type of widgets in the given areas,
1889 recognizing the type of icons in the given areas, and recognizing texts in the given areas. The
quality of the responses is measured by exact match accuracies.

1890
1891
1892
1893
1894
1895
1896
1897
1898
1899
1900
1901
1902
1903
1904
1905
1906
1907
1908
1909
1910
1911
1912
1913
1914
1915
1916
1917
1918
1919
1920
1921
1922
1923
1924
1925
1926
1927
1928
1929
1930
1931
1932
1933
1934
1935
1936
1937
1938
1939
1940
1941
1942
1943



Figure 11: Illustration of image grid selection used in dynamic image splitting for high-resolution image encoding. (Left) If the grid can cover the full image without scaling down, we choose the grid that minimizes padding. (Right) Otherwise, we choose the grid that minimizes the resolution loss due to scaling down.

Each of these two sets Ferret-UI tasks further have two variants with screenshots from two types of operating systems (iOS/Android), of which Android tasks are denoted as -A (e.g., Grd-A), and iPhone tasks as -i, which results in 12 tasks in total.

A.11 DYNAMIC VS STATIC IMAGE SPLITTING

Detailed ablation study of MM1.5 with different image splitting strategies is shown in Table 15, 16, 17 and 18. All models are using the final setting except for the image splitting (dynamic vs. static).

Table 15: Comparison of our models when using dynamic vs. static image splitting. We follow our final settings for all models. (S) and (D) indicate static and dynamic splitting, respectively.

Model	Knowledge Benchmarks				General Benchmarks					
	AI2D (test)	SQA (test)	MMMU (val)	MathV (testmini)	MME (P/C)	SEED ^l	POPE	LLaVA ^w	MM-Vet	RealWorldQA
<i>1B Model Comparison</i>										
MM1.5-1B(S)	59.5	83.9	36.1	37.4	1393.4/244.9	69.99	87.9	67.9	34.2	51.8
MM1.5-1B(D)	59.3	82.1	35.8	37.2	1365.7/245.7	70.2	88.1	71.6	37.4	53.3
MM1.5-1B-MoE(S)	66.4	86.8	41.2	42.2	1481.4/293.6	71.3	89.5	76.5	41.8	60.1
MM1.5-1B-MoE(D)	67.1	87.6	41.2	42.9	1511.9/361.1	71.4	88.6	75.5	39.8	57.8
<i>3B Model Comparison</i>										
MM1.5-3B(S)	66.1	87.2	36.8	43.1	1439.8/297.5	71.9	88.3	72.1	38.3	58.8
MM1.5-3B(D)	65.7	85.8	37.1	44.4	1478.4/319.6	72.4	88.1	73.0	41.0	56.9
MM1.5-3B-MoE(S)	66.3	89.3	41.9	43.1	1527.8/342.5	72.4	88.4	78.5	41.4	59.2
MM1.5-3B-MoE(D)	69.9	89.8	42.9	46.9	1591.4/365.7	73.3	87.2	76.1	43.7	60.7
<i>7B Model Comparison</i>										
MM1.5-7B(S)	72.2	89.6	44.1	49.1	1531.3/366.4	73.5	88.6	77.2	43.3	57.0
MM1.5-7B(D)	72.2	89.6	41.8	47.6	1514.9/346.4	73.4	88.6	74.2	42.2	62.5
<i>30B Model Comparison</i>										
MM1.5-30B(S)	75.4	92.8	46.8	56.0	1605.2/402.1	74.1	89.0	79.5	49.4	68.0
MM1.5-30B(D)	77.2	91.9	47.4	55.6	1646.2/405.7	75.0	88.6	80.4	52.0	69.0

A.12 METHODOLOGY FOR RUNNING COMPETITOR MODELS

This section covers the methodology used to report results for Phi-3-Vision (Abdin et al., 2024b), LLaVA-OneVision (Li et al., 2024c), InternVL2 (Chen et al., 2024b) and MiniCPM-V2 (Yao et al., 2024b). When available, we reported the results published by the original authors, either in their technical reports or on public leaderboards⁷. When not available, we implemented inference runners using publicly released checkpoints. Commonly, we followed (Li et al., 2024b)’s implementations that we adapted on our own internal fork of lm-eval-harness (Gao et al., 2023; McKinzie et al., 2024). To verify the validity of our inference implementations, we ensured we could reproduce previously published results within standard deviation. Below, we share details for each model implementation:

⁷https://huggingface.co/spaces/opencompass/open_vlm_leaderboard

Table 16: Comparison of our models when using dynamic vs. static image splitting. We follow our final settings for all models. (S) and (D) indicate static and dynamic splitting, respectively.

Model	Text-rich Benchmarks						
	WTQ (test)	TabFact (test)	OCRBench (test)	ChartQA (test)	TextVQA (val)	DocVQA (test)	InfoVQA (test)
<i>1B Model Comparison</i>							
MM1.5-1B(S)	31.0	65.4	60.4	67.5	72.8	79.7	40.8
MM1.5-1B(D)	34.1	66.1	60.5	67.2	72.5	81.0	50.5
MM1.5-1B-MoE(S)	34.1	69.6	58.0	72.7	75.8	82.5	46.0
MM1.5-1B-MoE(D)	38.9	71.4	62.6	73.7	76.1	84.8	55.9
<i>3B Model Comparison</i>							
MM1.5-3B(S)	36.3	71.0	61.1	74.3	75.2	84.0	45.8
MM1.5-3B(D)	41.8	72.9	65.7	74.2	76.5	87.7	58.5
MM1.5-3B-MoE(S)	32.5	70.1	60.2	73.0	75.9	81.0	44.2
MM1.5-3B-MoE(D)	39.1	73.1	63.8	73.6	76.8	85.0	53.6
<i>7B Model Comparison</i>							
MM1.5-7B(S)	38.4	73.7	59.7	77.9	76.1	84.5	47.3
MM1.5-7B(D)	46.0	75.9	63.5	78.6	76.5	88.1	59.5
<i>30B Model Comparison</i>							
MM1.5-30B(S)	46.0	81.0	64.5	82.4	78.7	88.5	53.2
MM1.5-30B(D)	54.1	84.0	65.8	83.6	79.2	91.4	67.3

Table 17: Comparison of our models when using dynamic vs. static image splitting. We follow our final settings for all models. (S) and (D) indicate static and dynamic splitting, respectively.

Model	Refer and Ground Benchmarks			
	RefCOCO avg.	Flickr30k (test)	LVIS avg.	Ferret-Bench avg.
<i>1B Model Comparison</i>				
MM1.5-1B(S)	82.0	82.7	62.4	69.7
MM1.5-1B(D)	81.4	83.0	62.2	67.4
MM1.5-1B-MoE(S)	79.3	80.9	63.9	73.4
MM1.5-1B-MoE(D)	84.8	85.4	64.6	69.6
<i>3B Model Comparison</i>				
MM1.5-3B(S)	85.1	85.3	68.1	71.2
MM1.5-3B(D)	85.6	85.9	67.9	69.5
MM1.5-3B-MoE(S)	82.8	82.6	67.5	70.8
MM1.5-3B-MoE(D)	86.2	85.8	66.9	72.2
<i>7B Model Comparison</i>				
MM1.5-7B(S)	87.2	86.0	68.8	71.2
MM1.5-7B(D)	86.6	85.3	66.4	72.6
<i>30B Model Comparison</i>				
MM1.5-30B(S)	90.1	87.7	73.2	75.6
MM1.5-30B(D)	90.1	87.5	73.1	77.1

Phi-3-Vision. We used the public Phi-3-Vision checkpoint⁸ and ran it on our families of benchmarks. For **general**, **text-rich**, **knowledge** and **refer&ground** benchmarks, when the position of the image is not determined by the task, we prepend the image to the text input following the examples given in the Phi-3-Vision cook book⁹. For **grounding** benchmarks, we introduced the following prompt: “Question: {question}Answer this question by listing the requested entities and their bounding boxes. The bounding boxes are formatted as follows: <x1,y1,x2,y2>, each value is between 0-{upper_bound}.<n>Answer:”. For both **referring** and **grounding**, we experimented with a variety of upper bound bounding boxes. Through our experiments, we noticed that an upper box of 1 yielded to

⁸<https://huggingface.co/microsoft/Phi-3-vision-128k-instruct>

⁹https://github.com/microsoft/Phi-3CookBook/blob/main/md/03.Inference/Vision_Inference.md#3-comparison-of-multiple-images

Table 18: Comparison of our models when using dynamic vs. static image splitting. We follow our final settings for all models. (S) and (D) indicate static and dynamic splitting, respectively.

Model	Multi-image Benchmarks					
	QBench2 (val)	Mantis (test)	NLVR2 (val)	MVBench	BLINK (val)	Muirbench (test)
<i>1B Model Comparison</i>						
MM1.5-1B(S)	65.8	48.4	78.6	46.1	41.9	34.0
MM1.5-1B(D)	66.4	50.7	79.0	45.8	46.3	34.7
MM1.5-1B-MoE(S)	70.2	52.1	83.0	47.4	44.8	42.5
MM1.5-1B-MoE(D)	70.9	51.2	83.2	48.3	43.7	40.9
<i>3B Model Comparison</i>						
MM1.5-3B(S)	72.0	53.5	83.9	47.8	42.5	44.5
MM1.5-3B(D)	73.2	54.8	83.8	47.7	46.8	44.3
MM1.5-3B-MoE(S)	70.4	54.4	85.3	47.2	47.1	44.2
MM1.5-3B-MoE(D)	73.8	54.4	86.0	50.3	49.8	45.6
<i>7B Model Comparison</i>						
MM1.5-7B(S)	73.0	56.7	87.2	49.7	47.6	53.8
MM1.5-7B(D)	73.2	57.6	86.9	48.3	48.2	49.1
<i>30B Model Comparison</i>						
MM1.5-30B(S)	77.0	64.5	90.2	49.9	48.4	60.1
MM1.5-30B(D)	79.3	64.6	90.6	54.0	50.2	58.2

better results, in line with the answers produced by Phi-3-Vision. For Flickr30k, we slightly simplified the benchmark and asked the model to ground one entity per prompt, as grounding multiple entities jointly did not lead to satisfactory results.

LLaVA-OneVision. We used the public checkpoint LLaVA-OneVision 7B¹⁰ and we followed closely the LLaVA documentation¹¹. When not baked directly into the benchmarks, we used the original LLaVA prompts specified in (Liu et al., 2023a; Li et al., 2024c) for all families of benchmarks. In particular, for **grounding** benchmarks, we used the prompt introduced in Table 18 of (Li et al., 2024c): “Provide the bounding box coordinate of the region this sentence describes”. On Flickr30k, we followed the single-entity approach outlined above.

InternVL2. The InternVL2 authors provided already a comprehensive set of benchmarks on **general, text-rich, knowledge** and **refer&ground** families¹², which we reported first. For the few remaining benchmarks, we used the 2B public checkpoint released. InternVL2 code base relies on both VLMEvalKit (Duan et al., 2024) and a custom internal evaluation¹³. We carefully reviewed the logic implemented¹⁴, especially regarding the decoding parameters and prompts used. For **grounding**, we used the prompt shared by the authors: “Please provide the bounding box coordinates of the region this sentence describes: <ref>{question}</ref>”. On Flickr30k, we followed the single-entity approach outlined above.

MiniCPM-V2. We used the publicly released MiniCPM-V2 2.8B checkpoint¹⁵. Similarly to InternVL2, MiniCPM-V2 code base relies on both VLMEvalKit and a custom internal implementation¹⁶, which we reviewed carefully to reproduce decoding parameters and prompts. For **refer&ground** benchmarks, we noticed that regardless of the prompt used, MiniCPM-V2 could not produce satisfac-

¹⁰<https://huggingface.co/lmms-lab/llava-onevision-qwen2-7b-ov>

¹¹https://github.com/LLaVA-VL/LLaVA-NeXT/blob/main/docs/LLaVA_OneVision_Tutorials.ipynb

¹²<https://huggingface.co/OpenGVLab/InternVL2-2B>

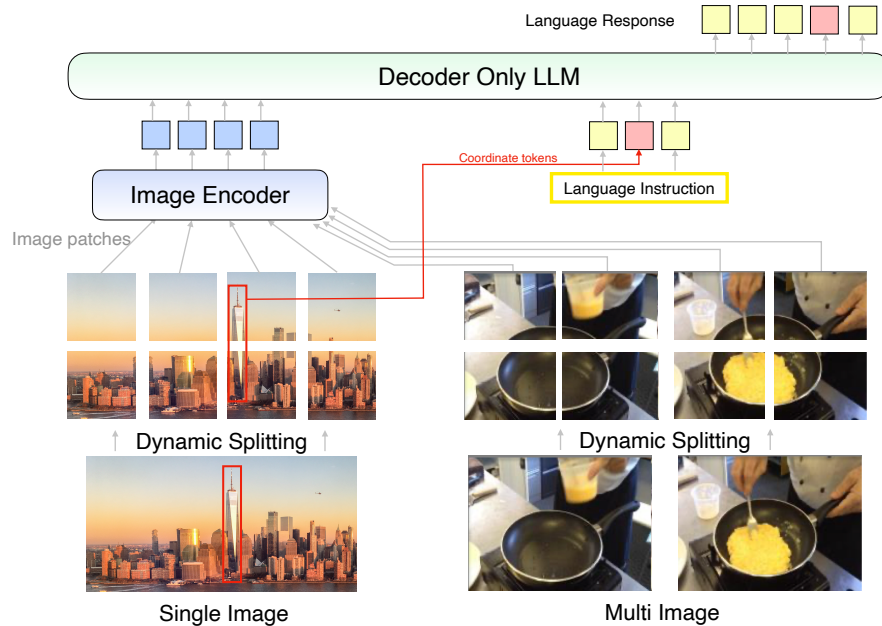
¹³<https://internvl.readthedocs.io/en/latest/internvl2.0/evaluation.html>

¹⁴<https://github.com/OpenGVLab/InternVL>

¹⁵<https://huggingface.co/openbmb/MiniCPM-V-2>

¹⁶https://github.com/OpenBMB/MiniCPM-V/tree/main/eval_mm

2052 tory results on RefCOCO and Flickr30k¹⁷. We decided not to include those results. For **multi-image**
 2053 and **in-context learning** benchmarks, we found that MiniCPM-V2 does not accept multiple images
 2054 as input in its Hugging Face implementation. We acknowledge MiniCPM-V2’s authors used a custom
 2055 image concatenating approach for BLINK¹⁸, but we could not reproduce easily the same approach on
 2056 other benchmarks. We decided to only include the BLINK score reported by the authors¹⁹.



2083 Figure 12: The overview of model architecture. MM1.5 excels at (i) text-rich image understanding
 2084 with dynamic image splitting, (ii) visual referring and grounding with coordinate tokens, and (iii)
 2085 multi-image reasoning.
 2086

2103 ¹⁷Responses commonly produced incomplete bounding boxes, preventing any parsing for a fair evaluation.

2104 ¹⁸https://github.com/OpenBMB/MiniCPM-V/blob/a209258d851f404485e5ae25864417dff3bb74ca/eval_mm/vlmevalkit/vlmeval/api/base.py#L260

2105 ¹⁹https://huggingface.co/spaces/opencompass/open_vlm_leaderboard

A.13 QUALITATIVE EXAMPLES

A.13.1 MM1.5 CAPABILITIES

Refer & Ground



What can I make with these ingredients <111,24,315,229> <308,235,460,314> <383,372,571,485>?

The ingredients <111,24,315,229> <308,235,460,314> <383,372,571,485> can be used to make a delicious cake. The first ingredient is cake flour, the second one is eggs, and the third one is butter. These are all essential components for baking a cake.

Should I add this stuff <101,306> to my cake too?

Yes, you should definitely add the canned cherries <54,211,165,388> to your cake. They will add a sweet and tangy flavor to the cake, enhancing its taste.

If we want to make a cake, choose the best ingredients in the image.


To make a cake, you would need flour, sugar, eggs, butter, and baking soda from the image.

Can you show me their coordinates?

Sure! The flour <112,26,316,239>, sugar <306,19,484,251>, eggs <312,239,392,312> <386,243,461,316>, butter <383,371,571,481>, and baking soda <457,155,567,308> are the ingredients you would need for a cake.



Multi-Image



Help me generate a Twitter post providing these images.

Step 1: Identify the main subject of each image.

- Image 1: The main subject is a crowd of people at a concert.
- Image 2: The main subject is the Sagrada Familia, a large Gothic-style church in Barcelona.
- Image 3: The main subject is a cup of coffee with a heart-shaped foam design.

Step 2: Determine the tone and theme of each image.

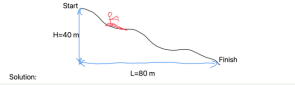
- Image 1: The tone is energetic and lively, with a focus on the vibrant atmosphere of a concert.
- Image 2: The tone is historical and architectural, showcasing the grandeur of the Sagrada Familia.
- Image 3: The tone is cozy and inviting, with a focus on the comforting act of enjoying a cup of coffee.

Step 3: Craft a Twitter post that incorporates the main subject and tone of each image.

"Experience the energy of a live concert at [Concert Venue] or take a moment to appreciate the architectural beauty of [Sagrada Familia] with [Tourist Attraction]. Enjoy a warm cup of coffee with a heart-shaped foam design from [Coffee Shop]."

Math/Reasoning

23. A skier slides down the frictionless slope as shown. What is the skier's speed at the bottom?



Solution:

Try to reason about the question step by step.

To find the skier's speed at the bottom, we can use the conservation of energy principle. At the start, the skier has potential energy, and at the end, the skier has kinetic energy. Since the energy is conserved, we can set up the following equation:

Start: $E = mgh$ End: $E = (1/2)mv^2$

where E is the energy, m is the mass of the skier, g is the acceleration due to gravity (9.81 m/s^2), h is the height, and v is the final velocity. We are given the initial height (40 m) and the final height (0 m) since the skier reaches the ground. We can plug these values into the equation and solve for the final velocity (v):

$$(1/2)mv^2 = mgh$$

Divide both sides by m:

$$(1/2)v^2 = gh$$

Now, plug in the given values for g and h:

$$(1/2)v^2 = (9.81 \text{ m/s}^2)(40 \text{ m})$$

$$(1/2)v^2 = 392.4 \text{ J}$$

Multiply both sides by 2:

$$v^2 = 784.8 \text{ J}$$

Now, take the square root of both sides to find the final velocity (v):

$$v = \sqrt{784.8 \text{ J}}$$

$$v \approx 28 \text{ m/s}$$

So, the skier's speed at the bottom is approximately 28 m/s.

MM1: Methods, Analysis & Insights from Multimodal LLM Pre-training

Brenden McKinzie*, Zhe Gan*, Jean-Philippe Fauconnier*, Sam Dodge*, Bowen Zhang*, Philippe Duhan*, Dhruv Shah*, Xuanhui Di*, Pratik Puri*, Pavan Waleel, Aron Hoi, Shaden Zhang, Kamran Shadi, Dong Kook, Anshu Jain, Hengyi Li, Max Schwarzer, Dan Guzman, Xiang Kong, Anson Zhang, Jinyu Wang, Cheng Wang, Nan Du, De Li, Sun Wanyun, Guo Yin, Mark Lee, Zhi Wang, Rowing Peng, Jovan Crnkic*, Alexander Tarlow*, and Yuhui Yang*

Apple
facebook@openai.com, the.gan@apple.com
*First authors; **Equal authors; ***Equal authors

Abstract: In this work we discuss building performant Multimodal Large Language Models (MLLMs). In particular, we study the importance of various architecture components and data choices. Through careful and comprehensive ablations of the image encoder, the vision language connector, and vision pre-training data choices, we identified several crucial design lessons. For example, we demonstrate that for large-scale multimodal pre-training using a variety of image sources, adversarial prompts, and text-only data is crucial for achieving state-of-the-art (SOTA) few-shot results across multiple benchmarks, compared to other published multimodal pre-training models. Further, we show that the image encoder together with image resolution and the image token count (the architectural input), while the vision-language connector design is of comparatively negligible importance. By scaling up the presented recipe, we build MM1, a family of multimodal models, including both dense variants up to 30B and mixture-of-experts (MoE) variants up to 64B. Our MM1s are SOTA in pre-training metrics and achieve competitive performance after applying our training on a range of established multimodal benchmarks. Thanks to large-scale pre-training, MM1 enjoys appealing properties such as enhanced in-context learning, and multi-image reasoning, enabling few-shot chain-of-thought prompting.

Text Rich

Read out the abstract of this paper.

In this work, we discuss building performant Multimodal Large Language Models (MLLMs). In particular, we study the importance of various architecture components and data choices. Through careful and comprehensive ablations of the image encoder, the vision language connector, and various pre-training data choices, we identify several crucial design lessons. For example, we demonstrate that for large-scale multimodal pre-training using a careful mix of image-captioning, the interleaved image-text and text-only data is crucial for achieving state-of-the-art (SOTA) few-shot results across multiple benchmarks, compared to other published multimodal pre-training results. Further, we show that the image encoder together with image resolution and the image token count has substantial impact, while the vision-language connector design is of comparable negligible importance. By scaling up the presented recipe, we build MM1, a family of multimodal models, including both dense variants up to 30B and mixture-of-experts (MoE) variants up to 64B, that are SOTA in pre-training metrics and achieve competitive performance after supervised finetuning on a range of established multimodal benchmarks. Thanks to large-scale pre-training, MM1 enjoys appealing properties such as enhanced in-context learning, and multi-image reasoning, enabling few-shot chain-of-thought prompting.

Figure 13: Examples of MM1.5 capabilities. The examples we demonstrated are generated by the MM1.5-3B model..

2160
2161
2162
2163
2164
2165
2166
2167
2168
2169
2170
2171
2172
2173
2174
2175
2176
2177
2178
2179
2180
2181
2182
2183
2184
2185
2186
2187
2188
2189
2190
2191
2192
2193
2194
2195
2196
2197
2198
2199
2200
2201
2202
2203
2204
2205
2206
2207
2208
2209
2210
2211
2212
2213

A.13.2 TEXT-RICH IMAGE UNDERSTANDING



Could you summarize every article on this newspaper page?

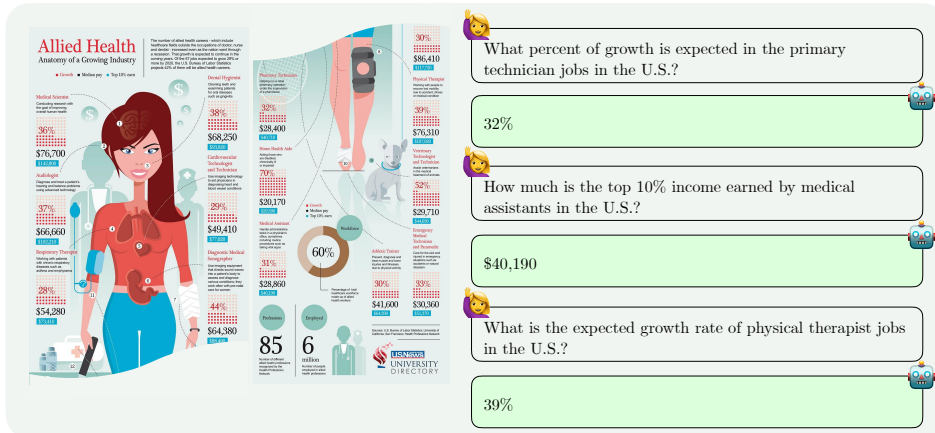
The newspaper page is from The New York Times dated November 11, 1918. The main headline announces the signing of the Armistice, marking the end of World War I. Other articles cover the revolution in Germany, with Berlin being seized by revolutionists and the abdication of Kaiser Wilhelm II. The page also includes a call for the abdication of the German Emperor by the socialist Chancellor, Friedrich Ebert. Additionally, there are reports on the ousting of Kaiser Wilhelm II and his flight to the Netherlands, as well as the resignation of the German General Staff. The page also features a report on the armistice being signed in France, marking the end of the war.



Could you summarize the articles in this newspaper page?

The newspaper page features several articles. The main headline reports on the tragic event of 60 people dying in blasts at US embassies. Another article discusses President Clinton consoling the victims' families. There's also a piece about Ojukwu foreclosing on a presidential ambition. Additionally, the page includes a special sales advertisement for Samsonite/Carlton luggage and high-quality crystals.

2214
2215
2216
2217
2218
2219
2220
2221
2222
2223
2224
2225
2226
2227
2228
2229
2230
2231
2232
2233
2234
2235
2236
2237
2238
2239
2240
2241
2242
2243
2244
2245
2246
2247
2248
2249
2250
2251
2252
2253
2254
2255
2256
2257
2258
2259
2260
2261
2262
2263
2264
2265
2266
2267



What percent of growth is expected in the primary technician jobs in the U.S.?

32%

How much is the top 10% income earned by medical assistants in the U.S.?

\$40,190

What is the expected growth rate of physical therapist jobs in the U.S.?

39%

Title	Sales	Series	Platform(s)	Initial release date
Minecraft	300,000,000	Minecraft	Multi-platform	November 18, 2011 ¹⁴
Grand Theft Auto V	200,000,000	Grand Theft Auto	Multi-platform	September 17, 2013
Wii Sports	82,900,000	Wii	Wii	November 19, 2006
PUBG: Battlegrounds	75,000,000	PUBG Universe	Multi-platform	December 20, 2017
Mario Kart 8 / Deluxe	71,360,000	Mario Kart	Wii U / Switch	May 29, 2014
Red Dead Redemption 2	65,000,000	Red Dead	Multi-platform	October 26, 2018
Terraria	58,700,000	None	Multi-platform	May 16, 2011
Super Mario Bros.	58,000,000	Super Mario	Multi-platform	September 13, 1985
Overwatch		Overwatch	Multi-platform	May 24, 2016
Human: Fall Flat	50,000,000	None	Multi-platform	July 22, 2016
The Witcher 3: Wild Hunt		The Witcher	Multi-platform	May 19, 2015
Tetris (Game Boy / NES)	48,000,000	Tetris	Game Boy / NES	June 14, 1989
Pokémon Red / Green / Blue / Yellow	47,520,000	Pokémon	Multi-platform	February 27, 1996
Animal Crossing: New Horizons	45,850,000	Animal Crossing	Nintendo Switch	March 20, 2020
Wii Fit / Plus	43,800,000	Wii	Wii	December 1, 2007
Pac-Man	42,000,000	Pac-Man	Multi-platform	May 22, 1980


Can you give me a table of games and sales numbers, but only show games released before 2010

Sure, here is a table of games released before 2010 and their sales numbers:

Title	Sales	Series	Platform(s)	Initial release date
Wii Sports	82,900,000	Wii	Wii	November 19, 2006
Super Mario Bros.	58,000,000	Super Mario	Multi-platform	September 13, 1985
Tetris (Game Boy / NES)	48,000,000	Tetris	Game Boy / NES	June 14, 1989
Pokémon Red / Green / Blue	47,520,000	Pokémon	Multi-platform	February 27, 1996
Pac-Man	42,000,000	Pac-Man	Multi-platform	May 22, 1980

2268
2269
2270
2271
2272
2273
2274
2275
2276
2277
2278
2279
2280
2281
2282
2283
2284
2285
2286
2287
2288
2289
2290
2291
2292
2293
2294
2295
2296
2297
2298
2299
2300
2301
2302
2303
2304
2305
2306
2307
2308
2309
2310
2311
2312
2313
2314
2315
2316
2317
2318
2319
2320
2321

A.13.3 VISUAL REFERRING AND GROUNDING



How to Pick a Perfect Watermelon

- Uniform Size & Heavy
- Elongated
- Orange Field Spot
- White Field Spot
- Larger "Webbing"
- Smaller "Webbing"
- Dark & Dull
- Shiny

Show me the guidelines for selecting the Ripe and Sweet melon

Uniform Size & Heavy: Pick a watermelon that is uniform in size and feels heavy for its size. This indicates that it is full of juice.

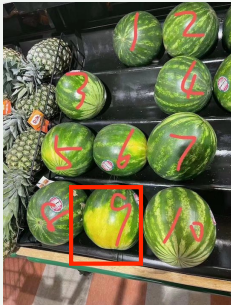
Larger "Webbing": Choose a watermelon with larger webbing, as it is likely to be sweeter.

Dark & Dull: A ripe watermelon will have a dark and dull exterior, which means it's ready to be enjoyed.

Field Spot: Look for a watermelon with a field spot, which is a yellow or orange spot on the bottom where it was resting on the ground. This indicates that it was allowed to ripen on the vine.


Orange Field Spot: The ideal watermelon will have an orange field spot, which means it was harvested at the perfect time.

Shiny: A ripe watermelon will not be shiny, so avoid any that are. By following these guidelines, you can select a ripe and sweet watermelon every time.



Based on the guidelines, which one is the ripe and sweet melon? Also show me the coordinates of the things that you mention.

The ripe and sweet melon <114,453,227,595> would be the one with a dark and dull exterior, an orange field spot, and larger webbing.





SUPERMARKET DEPARTMENTS

Which place should I go to if I want to buy lemons?

Fruits and Vegetables

Ok. Is this the correct place?

No, you are in the fresh meat area. The correct place to buy lemons is in the Vegetables department as shown in the supermarket image.

Okay, here is the place. Can you help me find the lemons? Also show me the coordinates of the things that you mention.

Sure! The lemons <236,218,646,448> are located in the middle of the image, nestled between the tomatoes and the peppers.

2322 A.13.4 MULTI-IMAGE REASONING
2323
2324
2325



2326
2327
2328
2329
2330
2331
2332
2333
2334 🧑
2335 In which of these situations can I drive on ahead?

2336
2337 🤖
2338 In the second image, you can drive on ahead because the traffic light is green.



2340
2341
2342
2343
2344
2345
2346
2347
2348 🧑
2349 What is the bike experiencing in image 1? Which one fits best, image 2 or image 3, and why?

2350
2351 🤖
2352 The bike in image 1 is experiencing rust and wear, as indicated by the rusted metal parts and the bent
2353 handlebars. Image 2, with its focus on the bicycle wheel, fits best as it provides a close-up view of the
2354 bike's wheel, which is the part most directly related to the bike's condition.




2355
2356
2357
2358
2359
2360
2361
2362
2363
2364
2365
2366
2367
2368
2369 🧑
2370 I have these ingredients in my fridge. What can I make using all of these? Explain.

2371
2372 🤖
2373 You can make a banana bread using all of these ingredients. The ripe bananas from image
2374 3 can be mashed and combined with the flour from image 1 and the eggs from image 4 to
2375 create a moist and flavorful banana bread. The chocolate chips from image 2 can be mixed
into the batter for added texture and sweetness.

2376 A.13.5 VIDEO UNDERSTANDING
 2377
 2378
 2379
 2380
 2381
 2382
 2383
 2384
 2385
 2386
 2387
 2388
 2389
 2390
 2391
 2392
 2393
 2394
 2395
 2396



2397 Here are two videos. Please provide the analysis on their differences.
 2398
 2399


2400 The first video and the second video are similar in that they both depict a person
 2401 gardening. However, there are some differences between the two videos. 

2402 In the first video, the person is seen picking berries from a bush, while in the second video,
 2403 the person is seen planting flowers in a garden. This difference in activity suggests that the
 2404 two videos may have been taken at different times or in different locations.

2405 Additionally, the first video is taken from a bird's-eye view, while the second video is taken
 2406 from a lower angle. This difference in perspective gives the two videos a different feel and
 2407 may affect the viewer's experience. Overall, while the two videos share some similarities,
 2408 they also have some differences in terms of the activity being performed and the perspective
 2409 from which the video is taken.




2417 Describe the player highlighted in this video.
 2418
 2419

2420 The highlighted player is a long jumper, who is wearing a green and black uniform and is 
 2421 participating a long jump competition.
 2422



2423 Why this player run very fast in the beginning of the video?
 2424
 2425

2426 The player runs very fast at the beginning of the video to gain momentum and speed for 
 2427 their jump, which will help them achieve a longer distance.
 2428
 2429

2430
2431
2432
2433
2434
2435
2436
2437
2438
2439
2440
2441
2442
2443
2444
2445
2446
2447
2448
2449
2450
2451
2452
2453
2454
2455
2456
2457
2458
2459
2460
2461
2462
2463
2464
2465
2466
2467
2468
2469
2470
2471
2472
2473
2474
2475
2476
2477
2478
2479
2480
2481
2482
2483



Describe the player highlighted in this video.

The player highlighted in this video is a gymnast. He is wearing a blue leotard and is shown performing on the parallel bars. The video captures his routine, which includes a variety of swings and movements on the apparatus. The gymnast's form and technique are on display as he navigates the parallel bars with precision and grace. The video also provides a close-up view of the gymnast's face, allowing viewers to see the concentration and determination he exhibits during his performance. Overall, the video showcases the gymnast's skill and dedication to his sport.



Do you think the player and his coach are satisfied with his performance?

The player and his coach are embracing each other in a sports hall or gym suggests a positive outcome or a sense of accomplishment, which could indicate satisfaction with the player's performance.



What was the primary objective that this person was trying to accomplish and what tool did he use repeatedly to check the accuracy of his work?

The primary objective that this person was trying to accomplish was installing or repairing a cable channel. He used a level repeatedly to check the accuracy of his work.

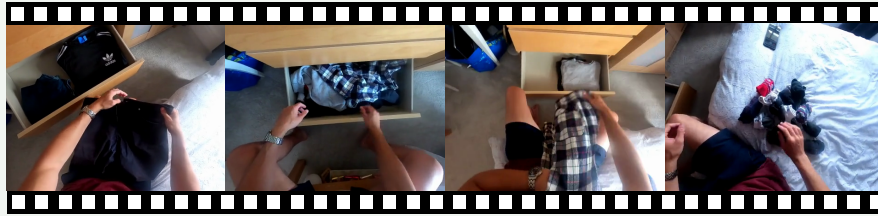


What activities did the man do after he washed the black pan?

He cleaned the kitchen counter and the sink with a white towel.

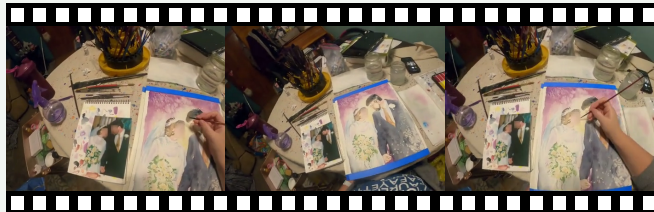


2484
2485
2486
2487
2488
2489
2490
2491
2492
2493
2494
2495
2496
2497
2498
2499
2500
2501
2502
2503
2504
2505
2506
2507
2508
2509
2510
2511
2512
2513
2514
2515
2516
2517
2518
2519
2520
2521
2522
2523
2524
2525
2526
2527
2528
2529
2530
2531
2532
2533
2534
2535
2536
2537



🧑 Please identify the most significant actions in the video. What conclusions can be drawn from these actions?

The character is seen lying on the bed, holding a black shirt. They then place the black shirt on the bed. The character is seen holding a gray shirt and places it on the bed as well. They then hold a pair of black socks and place them on the bed. The character is seen holding a pair of red socks and places them on the bed. The character is seen holding a pair of black shoes and places them on the bed. 🤖



🧑 Please describe the video in details.

In the video, a person is engaged in the act of painting a wedding scene on a canvas. The canvas is propped up on a table, which is cluttered with various art supplies. The person is holding a paintbrush, dipping it into a palette filled with different shades of paint. They are carefully applying the paint to the canvas, bringing the wedding scene to life. 🤖

The table around the canvas is a testament to the artist's process. It's covered in art supplies - brushes of different sizes and shapes, jars of paint in various colors, and a sketchbook filled with preliminary sketches. The sketchbook, in particular, provides a glimpse into the artist's thought process, with sketches of the wedding scene visible on its pages.

The background of the video is a wall adorned with shelves. The shelves are lined with more art supplies, indicating a well-stocked workspace. The overall scene suggests a dedicated artist immersed in their work, bringing a beautiful wedding scene to life on canvas.

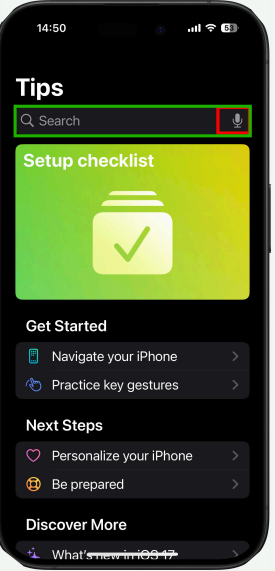
A.13.6 UI UNDERSTANDING

2538
2539
2540
2541
2542
2543
2544
2545
2546
2547
2548
2549
2550
2551
2552
2553
2554
2555
2556
2557
2558
2559
2560
2561
2562
2563
2564
2565
2566
2567
2568
2569
2570
2571
2572
2573
2574
2575
2576
2577
2578
2579
2580
2581
2582
2583
2584
2585
2586
2587
2588
2589
2590
2591



List all UI elements on the screen.

"UI widgets present in this screen include Text displaying "Projects" <16,48,103,81>, "more" Icon <273,48,303,79>, Text displaying "No Projects" <106,259,204,287>, Text displaying "Start New Project" <85,352,225,380>, "Magic Movie, Choose media from Photos and let iMovie create a movie for you." Button <0,413,310,482>, "Storyboard, Use beautiful templates to easily create a video or movie trailer." Button <0,487,310,558>, "Movie, Make a movie from scratch using media, from Photos and your camera." Button <0,568,310,637>."



What is the type of icon at <257,118,299,153> ?

microphone

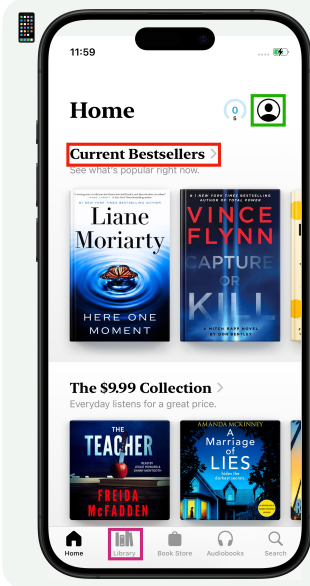
What happens if I click on it?

voice search

Is there another way to search?

Yes, you can also use the search field <10,118,303,155> at the top of the screen.

2592
2593
2594
2595
2596
2597
2598
2599
2600
2601
2602
2603
2604
2605
2606
2607
2608
2609
2610
2611
2612
2613
2614
2615
2616
2617
2618
2619
2620
2621
2622
2623
2624
2625
2626
2627
2628
2629
2630
2631
2632
2633
2634
2635
2636
2637
2638
2639
2640
2641
2642
2643
2644
2645



The screenshot shows the home page of an audiobook application. At the top, the time is 11:59. Below the status bar, there are icons for search and a profile. The main content is divided into two sections: 'Current Bestsellers' and 'The \$9.99 Collection'. The 'Current Bestsellers' section features two book covers: 'Liane Moriarty' and 'VINCE FLYNN'. The 'The \$9.99 Collection' section features two book covers: 'THE TEACHER' and 'A Marriage of LIES'. At the bottom, there is a navigation bar with icons for Home, Library, Book Store, Audiobooks, and Search. The 'Library' icon is highlighted with a red box. To the right of the screenshot, there are four text boxes with questions and answers, each accompanied by a small robot icon.

Please provide a brief description of the screenshot.

page displaying various books

Where can I find the current best booksellers?

You can find the current best booksellers by clicking on the 'Current Bestsellers' text <20,130,212,160>.

Where should I tap to sign in to my account?

You can sign in to your account by tapping on the 'person' icon <255,70,294,111>.

What will happen if I tap <66,603,118,650>?

Tapping on the 'Library' tab <66,603,118,650> will take you to your personal library where you can view all the books you have added.